

**Studies on the function and target-RNA recognition of RNA-binding proteins essential for mouse
germ cell differentiation**

Wright, Danelle

Doctor of Philosophy

March 2021

Department of Genetics

School of Life Science

The Graduate University for Advanced Studies,

SOKENDAI

Table of Contents

Summary	p. 3
Introduction	p. 6
Chapter 1	
1.1 Background	p. 8
1.2 Materials and Methods	p. 9
1.3 Results	p. 15
1.4 Discussion	p. 22
Chapter 2	
2.1 Background	p. 27
2.2 Materials and Methods	p. 28
2.3 Results	p. 30
2.4 Discussion	p. 35
Thesis Conclusion	p. 40
Acknowledgements	p. 41
References	p. 42

Summary

Post-transcriptional regulation by RNA-binding proteins (RBPs) is highly important to establish gene regulatory networks during all stages of germ cell development. RBPs generally make functional complexes to control their target mRNA, but what kind of protein structures are needed to form these complexes and bind specific mRNA are largely unknown. One family of RBPs that is essential for germ cell development is NANOS. My studies focused on murine NANOS2 and NANOS3, which have different yet critical functions. NANOS3 is required for protection from apoptosis during migration and gonadal colonization of primordial germ cells (PGCs) in both sexes, whereas NANOS2 is male-specific and required for male-type differentiation of germ cells. What is interesting about these proteins is their reported one-way functional redundancy, i.e., NANOS2 can rescue NANOS3 function but NANOS3 cannot promote the male pathway. These two proteins are structurally similar, both having a conserved zinc finger domain and similar N-terminal. In the case of NANOS2, this zinc finger domain is required to interact with its partner, DND1. The other key protein domain, the N-terminal, is required for interaction with CNOT1 of the CCR4-NOT deadenylation complex. Previous studies demonstrated that NANOS2 and DND1 colocalize with processing body (P-body) components, such as CNOT1, in germ cells. NANOS2 carries out some of its post-transcriptional regulatory activity by targeting specific mRNA to these P-bodies. If the binding between DND1 and NANOS is inhibited, as in NANOS2 zinc finger mutant mice, these specific P-bodies are not formed and the male pathway does not proceed. However, although there are many reports of the phenotypes of such mutant mice, no study has looked at the dynamic process of events leading to P-body formation by germ cell-specific RBPs. Furthermore, in *Nanos2*-knockout germ cells, up-regulated NANOS3 instead localizes with DND1 to these P-bodies in germ cells, but cannot rescue NANOS2 function, and it is unknown what its role is during this male differentiation stage. The purpose of my thesis study was to therefore clarify the role of NANOS2 in P-body-mediated RNA

regulation and reveal why NANOS3 is unable to substitute.

In the first chapter, I report my results obtained using conditional *Nanos3/Nanos2* knockout mice and chimeric mice expressing chimeric NANOS protein constructs to assess why NANOS3 cannot rescue NANOS2 function. These *in vivo* analyses demonstrated NANOS3 to be a “weaker” version of NANOS2 with inhibitory action against apoptosis. My study also suggested that mouse NANOS3 is different from human NANOS3 in that it cannot bind CNOT1, which is a reason for its inability to promote the male pathway through P-bodies. It is unknown whether human NANOS3 can promote the male pathway, but human NANOS3 may have stronger regulatory ability than mouse NANOS3. Using the unique and time-saving characteristics of chimera analysis, I additionally found that DND1 and NANOS2 binding is highly dependent on the specific NANOS2 structure itself, which is why NANOS3 has weaker binding with DND1, making it unable to regulate target mRNA to promote the male pathway.

Although I determined that the specific NANOS2 structure is a key point in its interactions with other proteins, the dynamic events leading to the formation of an individual P-body remained unclear. This question led to my second aim: to reveal how NANOS2 and DND1 interact with target mRNA and P-body components in real time. I decided to use live imaging techniques to analyze their interactions. In the second chapter, I report my achievement of establishing a system to view mRNA in real time using dCas13, an endonuclease-dead RNA-specific RNase. I also used two different mouse cultured cell lines to investigate P-body formation and mRNA targeting in the presence or absence of the germ cell-specific NANOS2 and DND1. The target mRNA visualized was *Dazl*, one of two known NANOS2 targets. In my cultured cell system, I was able to visualize the targeting of *Dazl* to P-bodies within 6 hours after inducing the expression of NANOS2 and DND1. I next compared *Dazl* localization under multiple conditions with wild-type and mutant NANOS2 and DND1. Based on the time-lapse imaging under all conditions, I proposed the following model of the events leading to mRNA regulation by NANOS2 and DND1: In the

presence of NANOS2, DND1 binds a specific target, in this case *Dazl*. NANOS2 then binds *Dazl*-bound DND1, bringing with it CNOT1 of the CCR4-NOT complex. This accumulation of components then likely reaches a threshold and induces phase separation for an energetically favorable configuration to form spherical P-bodies.

In conclusion, my thesis study revealed the specific structural basis for NANOS2 function in P-body-mediated RNA regulation, as well as the effects of its expression on the localization of other involved proteins and target mRNA. Determining how RBPs regulate their targets is highly important in understanding the downstream pathways in development. By combining new *in vivo* analyses, I was able to shed light on this highly intricate mechanism.

Introduction

In animals that reproduce through sexual reproduction, the development of functional germ cells is crucial in order to pass along genetic information to the next generation. RNA-binding proteins (RBPs) play major roles in regulating correct germ cell development (Licatalosi, 2016). These proteins generally make functional complexes; however, what kind of protein structures are needed to form these complexes and bind specific mRNA are largely unknown. One family of RBPs that is essential for germ cell development is NANOS. There are three NANOS homologues in the mouse: NANOS1 was found to be expressed in the central nervous system, but no phenotype for germ cell development was observed when it was knocked-out (Haraguchi et al., 2003). NANOS3 is expressed in the primordial germ cells (PGCs) to protect them from apoptosis during migration to the future gonad in both sexes, whereas NANOS2 is male specific and needed for male germ cell differentiation (Suzuki et al., 2007; Tsuda, 2003). These two proteins become expressed again during spermatogenesis, where NANOS2 is expressed in spermatogonial stem cells and NANOS3 is expressed in later aligned spermatogonia (Lolicato et al., 2008; Sada et al., 2009). Previous reports showed that NANOS3 is expressed in the primordial germ cells to protect them from apoptosis during migration to the future gonad in both sexes. NANOS2, however, is male specific and needed for male germ cell differentiation (Suzuki et al., 2008; Tsuda et al., 2003). These two proteins are structurally similar, both having a conserved zinc finger domain and similar N-terminal. In the case of NANOS2, this zinc finger domain is needed for interaction with the recently discovered partner of NANOS2, DND1 (Suzuki et al., 2016). Another key protein domain is the N-terminal, which is needed for interaction with the CCR4-NOT complex (Suzuki et al., 2012). NANOS2 and DND1 binding is necessary to recruit target RNAs. Once RNA is bound, NANOS2, DND1, CCR4-NOT, and other proteins form processing bodies (P-bodies), which are granules for RNA degradation/storage that form through phase separation. Currently, the functions and formation mechanisms of P-bodies are unclear (Aizer et al.,

2008), and many studies have focused on elucidating their properties among cell types and in comparison with other ribonucleoprotein granules such as stress granules (Decker and Parker, 2012; Stoecklin and Kedersha, 2013). Binding of DND1 and NANOS is required for this process of P-body formation (Suzuki et al., 2016). In the absence of NANOS2, NANOS3 is upregulated and localizes with DND1 to these P-bodies, but NANOS3 cannot rescue NANOS2 function, and its role during this male differentiation stage is unknown. My studies therefore focused on two different yet related questions regarding NANOS-mediated promotion of germ cell development: 1) What is the role of NANOS3 during this male differentiation stage and why is it unable to rescue NANOS2 function, and 2) what are the individual roles of NANOS2 and DND1 in the process of P-body formation? In Chapter 1, I will describe my study of the role of NANOS3 in the male differentiation stage. In Chapter 2, I will discuss my examination of the interactions among NANOS2, DND1 and target mRNA. Based on my research, NANOS3 is needed to protect germ cells from apoptosis in the absence of NANOS2 even though it cannot promote male germ cell differentiation, which is caused by its weaker affinity for DND1, making it unable to regulate target mRNA. In addition, I revealed the distinct roles of DND1 and NANOS2 in the targeting of specific mRNA to P-bodies using a new method for live imaging of RNA. This thesis describes the results of these related studies and discusses some future questions to be addressed.

Chapter 1

1.1 Background

As stated in the introduction, the NANOS family of RBPs plays major roles in germ cell development. NANOS proteins are structurally similar in that they have a conserved zinc finger domain (ZF) and similar N-terminal. In the case of NANOS2, the ZF domain is needed for interaction with its recently discovered partner, dead end 1 (DND1)(Suzuki et al., 2016). DND1 is an RBP conserved among vertebrates that is important for the survival of PGCs and functions in numerous RNA regulatory processes in germ cell development (Gross-Thebing and Raz, 2020). Suzuki et al. previously reported that the loss of DND1 results in the loss of association between NANOS2 and its target RNA (Suzuki et al., 2016). Moreover, they reported that mutation of the CCHC-CCHC motif of the zinc finger domain prevents DND1 binding. The other key protein domain, the N-terminal, is needed for interaction with the CCR4-NOT deadenylation complex, specifically by binding the component CNOT1 (Suzuki et al., 2014, 2012). NANOS2 directly binds CNOT1, and NANOS2 and DND1 binding is necessary to recruit target RNAs. NANOS2, DND1, CCR4-NOT and other proteins form P-bodies. In male germ cells, the formation of these specific NANOS2-DND1 P-body-like granules may be essential for male differentiation to proceed.

If *Nanos2* is knocked out, several characteristic phenotypes are observed in the embryonic testes that lead to the eventual sterility of male mice. First, germ cells fail to express DNMT3L, a methyltransferase required for establishing male-type DNA methylation, and other markers for male germ cell differentiation (Suzuki and Saga, 2008). Instead, *Nanos2*-null gonocytes begin to express the normally repressed transcription factor STRA8, by which they abnormally enter meiosis and eventually die due to apoptosis (Suzuki et al., 2016; Suzuki and Saga, 2008; Tsuda, 2003). Moreover, NANOS3, which is down-regulated following the start of NANOS2 expression at around E13.5, becomes highly expressed in the

absence of NANOS2 (Suzuki et al., 2007). Of note, although ectopic NANOS2 was reported to rescue the functions of NANOS3 in PGCs in early development, NANOS3 cannot rescue the later NANOS2 function for male differentiation even though it becomes up-regulated in *Nanos2*-null germ cells (Tsuda, 2003). However, it is unknown whether NANOS3 plays any role during this sexual differentiation stage in mouse germ cells.

Thus, using conditional *Nanos3/Nanos2* double knockout mice and chimeric mice expressing chimeric NANOS protein constructs created via CRISPR/Cas9 technology, I attempted to clarify the roles and structural basis underlying the functional redundancy of NANOS proteins. The content of this study was published in 2020. (Wright et al., 2020)

1.2 Materials and Methods

Mice

Mice were housed in a specific-pathogen-free animal care facility at the National Institute of Genetics. All experiments were approved by the NIG Institutional Animal Care and Use Committee. *Nanos2-mcherry*, *Nanos3 cKO* mice were generated by ES-mediated homologous recombination. All mouse lines used in this study were of a mixed genetic background.

Production of Nanos2-mCherry mice

This line was derived from the *Nanos2 cKO* mouse line produced as follows: For the targeting vector construction, homologous arms and 3xFlag-*Nanos2* were prepared by PCR amplification from the mouse genome and 3x-Flag-*Nanos2*-cDNA construct previously reported (Suzuki and Saga, 2008), and were integrated into the DT-ApA/conditional KO FW vector containing the *loxP*, *Frtd*, and *Pgk*-neomycin cassette (<http://www.cdb.riken.go.jp/arg/cassette.html>). The mCherry cassette was integrated

after the 3' loxP site just before the *Nanos2*-3'UTR. To facilitate homologous recombination, Cas9 target sites were selected using CRISPR direct (<http://crispr.dbcls.jp/>) and the target sequence (5'-GGGTTGCATCTTGTTACATA-3') was integrated into the px330 Cas9 vector (Addgene). The targeting vector and the Cas9 vector were transfected into TT2 ES cells, and the homologous recombinants were selected using 150 µg/ml neomycin-containing medium. Correctly recombined ES cells were screened using the following primer sets: Nanos2-cKO-L1 (5'-TATGTAACAAGATGCAACC-3') and FLAG-R (5'-CACCGTCATGGTCTTTGTAGTCG-3') for 5' recombination, and CAT-pA-L4 (5'-CCTCTACAAATGTGGTATGGCTG-3') and N2-H2(H1?) (5'-CCTGCAACTCTGTAGACTAGGCTGGCC-3') for 3' recombination. These ES cells were aggregated with 8-cell embryos, and the blastocysts that formed the next day were transferred to foster mothers to generate chimeric mice. After confirming germline transmission, the neomycin cassette was removed by crossing with *Rosa-Flp* mice (Dymecki, 1996). To create *Nanos2^{mcherry}*, the mice were crossed with CAG-Cre mice to remove *3xFlag-Nanos2*, as shown in Fig. 1A.

Production of Nanos3 conditional knockout mice

For targeting vector construction, the homologous arms and exon-1 part of *3xFlag-Nanos3* were prepared by PCR amplification from the mouse genome and 3xFlag-Nanos3 cDNA construct, and integrated into a vector containing two *loxP* sequences via the sequential infusion method (Yamane et al., 2018). Two Cas9 target sites were selected using CRISPR direct (<http://crispr.dbcls.jp/>), and each target sequence (5'-AAGGAAGTTGGAGCCAGGTT-3' and 5'-TCTGTTTGCCACTGGGTGCG-3') was integrated into the px330 Cas9 vector (Addgene) containing the PGK-puromycin cassette. These vectors were transfected into ES cells established from the Rosa-CreERT mouse line using Lipofectamine 2000 (Invitrogen) and homologous recombinants were selected using 1 µg/ml puromycin-containing medium

for the first 2 days. Correctly recombined ES cells were screened using the following primer sets: Nanos3-5'-UTR-F2 (5'- GGCATACTCTGCCCCCAACC -3') and FLAG-R (5'- CACCGTCATGGTCTTTGTAGTCG-3') for 5' recombination, and Lox-L1 (5'- GGACGTAAACTCCTCTTCAGACC -3') and Nanos3-PC1 (5'- GACCCTCGCTGGGTTCCCAG-3') for 3' recombination. I obtained an ES cell line that had a homozygously recombined *Nanos3-flox* allele. The ES cell line was aggregated with 8-cell embryos to generate chimeric mice as described above. The schema for creating *Nanos3* cKO mice is shown in Fig. 1B

Creation of conditional Nanos2/Nanos3 double knockout mice

A male *3xFlag-Nanos3^{flox/flox}/Rosa CreER^{T2}* chimeric mouse was crossed with female *Nanos2^{mcherry/mcherry}* mice to produce conditional *Nanos2/Nanos3* double knockout offspring by injecting tamoxifen at E11.5 to induce Cre recombination. Using this mouse line, single conditional *Nanos3* knockout, single *Nanos2* knockout, and double knockout mice were obtained. Genotypes were confirmed by PCR. *3xFlag-Nanos3^{flox/flox}/Nanos2^{+/mcherry}* mice negative for *Rosa CreER^{T2}* were considered as controls. Testes for each genotype were collected at embryonic day (E) 13.5-16.5, fixed in 4% PFA for 30 min, cryoprotected with sucrose, embedded in OCT compound, and frozen at -80°C until analysis.

Creation of mutant NANOS protein-expressing chimeric mice

To evaluate the functional domains of NANOS proteins, I created mutant constructs by interchanging the DNA domains encoding the N-terminal and ZF of NANOS2 and NANOS3. NANOS3 has a longer C-terminal than NANOS2. The extra C-terminal sequence (46 amino acids) was deleted such that it was the same length as that of NANOS2. The final two DNA constructs, 3xF-Nanos2N58-Nanos3ZF(Δ C46) and 3xF-Nanos3N54-Nanos2ZF, were respectively knocked into the *Nanos2* locus in mouse embryonic stem

(ES) cells using CRISPR/Cas9 gene editing (Cong et al., 2013). Homozygously mutated ES cells for each construct were aggregated with 8-cell mouse embryos to create chimeras. Chimeric testes were collected from E15.5, prepared as above, and immunohistochemically analyzed for male germ cell differentiation.

Immunohistochemistry

Frozen samples were cut into 5- μ m-thick slices and placed on coated glass slides. The slides were autoclaved at 105°C for 15 for antigen retrieval in Target Retrieval Solution (Dako). After rinsing with phosphate-buffered saline (PBS), the slides were blocked with 3% skim milk in PBS containing 0.1% Tween® (PBST) for 1 hr at room temperature (RT). The slides were then incubated with the following antibodies in Can Get Signal (Toyobo) at 4°C overnight: Anti-FLAG-HRP (Sigma, dilution 1/1000, #A8592), anti-DND1 (gift from Dr. Suzuki), anti-Rck/p54 (DDX6; MBL, dilution 1/300), anti-Ki-67 (Thermo, dilution 1/200, #RM-9106-S0), anti-STRA8 (gift from Dr. Ishiguro), anti-DNMT3L (gift from Dr. Yamanaka), anti-E-Cadherin (R&D Systems, dilution 1/500, #AF748), anti-NANOS3, anti-DAZL (Abcam, dilution 1/300, #ab34139), anti-cleaved PARP (Cell Signaling, dilution 1/300, #9548) and anti-SOX9 (Santa Cruz, dilution 1/300, #sc-20095). The slides were washed 3 times with PBST and incubated with the respective secondary antibodies conjugated with Alexa Fluor 488, 594 or 647 (Invitrogen) in PBST for 90 min at RT. After washing with PBST and PBS, the slides were stained with 4',6-diamidino-2-phenylindole (DAPI) and coverslips were mounted. For anti-FLAG-HRP staining, slides were incubated for 10 min in 3% hydrogen peroxide/ PBS to stop endogenous peroxidase activity before autoclaving. To detect HRP, the TSA kit (Perkin Elmer) was used following the manufacturer's instructions. Slides were imaged using an Olympus FV1200 confocal microscope. The obtained fluorescence images were analyzed using the ImageJ package Fiji (Schindelin et al., 2012).

Western blotting

Samples were boiled in 2x sample buffer for 5 min and run on gels for sodium dodecyl sulfate-polyacrylamide gel electrophoresis (SDS-PAGE). They were then transferred to PVDF (Immobilon) membranes. Membranes were blocked in 5% skim milk/ PBST for 1 hr at RT. They were then incubated with the primary antibodies overnight at 4°C. After washing 3 times with PBST, membranes were incubated with HRP-conjugated secondary antibodies for 1 hr at RT. Protein bands were visualized using SuperSignal™ West Femto Maximum Sensitivity Substrate (Thermo Scientific).

Protein stability analysis

Protein stability was assessed using cultured HEK293T cells (ATCC)(transfected with expression vectors for HA-DND1 alone or together with 3xF-NANOS2, -NANOS3, or –NANOS2-3C) and doxycycline-inducible ESCs. ESCs were established using the PiggyBac system (Yamane et al., 2018) and expressed 3xF-NANOS2-t2a-HA-DND1 upon doxycycline addition. Cells were cultured with or without cycloheximide, and cell lysates were used for Western blotting with anti-HA (Santa Cruz, dilution 1/2000, #sc-805), anti-FLAG-HRP (Sigma-Aldrich, dilution 1/10000, #A8592) and anti-β-tubulin, Sigma-Aldrich, dilution 1/4000, #T4026).

DND1-NANOS binding analysis

NANOS-DND1 binding was examined using cultured HEK293T cells (ATCC)(transfected with expression vectors for HA-DND1 and FLAG-NANOS2, -NANOS3, or the mutant proteins used in the chimera analysis. Forty-eight hours after transfection, cell lysates were used for immunoprecipitation with anti-FLAG (M2)(Sigma) agarose beads. Co-precipitated DND1 was evaluated by Western blotting with anti-HA (Santa Cruz, dilution 1/2000, #sc-805) and anti-FLAG-HRP (dilution 1/10000) antibodies.

NANOS single point mutants were created using site-directed mutagenesis (Laible and Boonrod, 2009). HEK293T cells were transfected with expression vectors for HA-DND1 and FLAG-NANOS2 single point mutants (I60L, N62S, Q78V, V87L, L98Q or Y111F) or NANOS3 point mutants (L56I, S58N, F107Y, all 3 mutations or all 6 mutations) using PEI methods. Forty-eight hours after transfection, cells were collected and lysates were used for immunoprecipitation as above.

Gluthione-S-transferase (GST) pull-down for CNOT1-NANOS direct binding

MBP-fused full-length mouse NANOS2, NANOS3, and GST-CNOT1-3 expressing *E.coli* were generously provided by Dr. Suzuki (Suzuki et al., 2014). CNOT1-3 refers to the C-terminal portion of the CNOT1 protein, which is where NANOS2 reportedly binds (Suzuki et al., 2014). To create MBP-fusion human NANOS3 NIM (huNANOS3-NIM) and MBP-fusion mouse NANOS3 NIM (mNANOS3-NIM) proteins, oligonucleotides encoding the respective NIM domains were annealed and ligated into the pMALc2 vector (Addgene) (Bhandari et al., 2014). BL21(DE3) *E.coli* were transformed with each pMAL construct and resulting clones were confirmed by DNA sequencing. MBP-fusion protein expression was induced by the addition of IPTG following the manufacturer's instructions. MBP-NANOS2, MBP-NANOS3, MBP-mNANOS3-NIM, MBP-mNANOS3-NIM N-D and MBP-huNANOS3-NIM were affinity purified using amylose resin (NEB), and proteins were confirmed by Western blotting with anti-MBP (NEB, 1/10000, E8032S). GST-CNOT1-3 protein expression was induced following previously reported methods (Suzuki et al., 2014). Each purified MBP-fusion protein was mixed with GST-CNOT1-3-expressing *E.coli* lysate and rotated at 4°C for 1.5 hrs. Protein mixtures were added to Gluthione Sepharose 4B beads (Amersham Biosciences) and rotated at 4°C for 2 hrs. Beads were washed and boiled with loading buffer for subsequent SDS-PAGE and Western blotting. CNOT1-3 expression was confirmed by Coomassie Brilliant Blue (CBB) staining.

Statistical analysis

To quantify immunofluorescence, signals on testis sections stained on the same slide from 3 embryos for each genotype were measured in Fiji. Cell counts were also similarly performed using Fiji. Significant differences between genotypes were assessed using the unpaired Student's t-test with Graphpad Prism 8. The error bars indicate S.D. A P-value of <0.05 was considered significant.

1.3 Results

Male differentiation proceeds normally without NANOS3

Previous studies revealed that NANOS3 is needed in PGCs to protect them from apoptosis as they migrate to the future gonad. However, its functions in later stages remain unclear. In males, its expression is downregulated after embryonic day (E)13.5 (Suzuki et al., 2007), and it becomes expressed again during spermatogenesis after birth (Lolicato et al., 2008; Sada et al., 2009). As the amount of NANOS3 protein is low in embryonic male germ cells after NANOS2 becomes expressed (Suzuki et al., 2007), no studies have examined whether the complete loss of NANOS3 during this interval affects germ cell development. Therefore, to address this, *Nanos3* conditional knockout mice were created here with help from the mouse unit. Pregnant *3xFlag-Nanos3^{flox/flox}/Nanos2^{+mcherry}/Rosa CreER^{T2}* mice were injected with tamoxifen at E11.5, and embryos were collected at E13.5-E15.5. There was no FLAG-NANOS3 expression in E13.5 germ cells, confirming efficient Cre-mediated recombination (Fig. 1C). Cre-negative embryos were used as controls. At all time points, there was no difference in the number of germ cells between control and *Nanos3* cKO embryos (Fig. 2A, B). Furthermore, expression of the male marker DNMT3L was observed,

suggesting that the male pathway was successfully initiated (Fig. 2C). However, protein expression of the NANOS2 target, DAZL (Kato et al., 2016), was increased in the *Nanos3* cKO embryos compared with control embryos even though NANOS2 was expressed. (Fig. 2D, E). This suggests that NANOS3 has some potential to repress certain NANOS2 targets, possibly being a “weaker” form of NANOS2.

NANOS3 protects germ cells from apoptosis in the absence of NANOS2

NANOS3 becomes abnormally upregulated in *Nanos2* KO-germ cells. However, the function of this high NANOS3 expression was unclear because it was previously unable to be compared with the *Nanos2/3* dKO condition. Of note, in the presence of a NANOS2 zinc finger mutant, NANOS3 does not become upregulated and the cells exhibit a more severe fate than *Nanos2* KO cells, including germ cell death by E18.5 (Suzuki et al., 2016), suggesting that NANOS3 also exhibits slight functional redundancy in the absence of NANOS2. In consideration of this, to assess the fate of germ cells in the absence of both NANOS proteins, *Nanos2/3* dKO mice were created here with help from the mouse unit.

Pregnant *3xFlag-Nanos3^{flox/flox}/ Nanos2^{mcherry/mcherry}/ Rosa CreER^{T2}* mice were injected with tamoxifen at E11.5, and embryos were collected at E13.5-E16.5. Cre-negative embryos were used as controls. At E13.5, there was no significant difference in the number of germ cells between dKO and control embryos, as I observed in the single *Nanos3* cKO (Fig. 2A, Fig. 3A, B). However, few germ cells remained the following day at E14.5, and by E15.5, the embryonic gonads were mostly devoid of germ cells (Fig. 3A, B), suggesting their rapid death. To check whether the cells were dying by apoptosis, testis sections were stained for cleaved PARP (cPARP). I compared dKO testes with wild-type and *Nanos2* KO testes at E14.5, but the number of cPARP signals in the dKO was higher, reflecting the more severe phenotype (Fig. 3C, D). Therefore, the dKO germ cells likely entered apoptosis soon after the E13.5 stage. *Nanos2* KO germ cells also die by apoptosis after E15.5, probably due to the abnormal cell cycle

regulation indicated by the up-regulation of STRA8 and resumption of mitotic activity (Suzuki and Saga, 2008). To assess if the dKO germ cells showed more severe cell cycle abnormality as expected by the rapid death, E14.5 testis sections were stained for STRA8 to mark meiosis and Ki-67 to mark the active cell cycle. In *Nanos2* KO mice, germ cells express STRA8, whereas its expression is suppressed in wild-type cells except in some cells near the mesonephros where the retinoic acid level is high. However, the dKO cells that were still alive had only weak or no expression of STRA8, being similar to the control (Fig. 3E). E14.5 dKO germ cells were positive for Ki-67, suggesting that the cell cycle was activated. This was in contrast to the control and *Nanos2* KO, in which the cell cycle is arrested, albeit only temporarily at E14.5 in the *Nanos2* KO case, in a large proportion of germ cells (Saba et al., 2014) (Fig. 3F). Therefore, in the absence of NANOS2, NANOS3 may suppress apoptosis by regulating genes related to the cell cycle. Furthermore, based on the lack of STRA8 expression, these remaining dKO cells were not entering meiosis. As *Nanos2* KO germ cells highly express NANOS3 and STRA8, NANOS3 may promote the abnormal meiotic entry of male embryonic germ cells.

NANOS2 is required for the maintenance of DND1 protein expression in vivo

One of the main mechanisms by which NANOS2 carries out its functions is by binding its partner DND1 and target RNA to form P-bodies. In *Dnd1* cKO germ cells, although no P-bodies are formed, the amount of NANOS2 protein is unchanged (Suzuki et al., 2016). In contrast, in my *Nanos2/3* dKO mice, the few remaining germ cells had lost the expression of DND1. DND1 was normally expressed at E13.5 (Fig. 4A), but was lost by E14.5 in *Nanos2/3* dKO germ cells (Fig. 4A). Reduced DND1 expression was also observed in *Nanos2* KO, but not in *Nanos3* KO germ cells at E14.5 (Fig. 4B). As the *Dnd1* mRNA level does not differ between wild-type and *Nanos2* KO germ cells at E14.5 (Fig. 4C) (Butler et al., 2018; Shimada et al., 2020 preprint), DND1 may be stabilized by strong binding to NANOS2. To assess the

protein stability of DND1, HEK293T cells were transfected with constructs for HA-DND1, FLAG-NANOS2 or NANOS3, and then treated with cycloheximide to inhibit translation. The cell lysates were collected at several time points after cycloheximide treatment and used for Western blotting. There was no difference in DND1 protein when it was expressed alone or with NANOS2 or 3 (Fig. 5A, B). However, I found that the NANOS2 protein level decreased over time in the cultured cells. To examine if the cell type and/or transient expression affected DND1 stability, the same experiment was performed using ES cells containing doxycycline-inducible *FLAG-NANOS2* and *HA-DND1* transgenes. However, similar to in HEK293T cells, DND1 protein was stable (Fig. 5C).

The NANOS2 ZF and N-terminal are both needed for male-type differentiation

Based on dKO analyses, the absence of both NANOS proteins causes the rapid loss of germ cells. In *Nanos2 KO* germ cells, NANOS3 is upregulated, enabling the germ cells to survive for a longer period, but male-type differentiation does not occur. To understand the mechanism underlying the uneven functional redundancy, I looked closer at the structure of the proteins themselves. NANOS3 has a similar CCHC-CCHC ZF domain to NANOS2 and is able to localize to P-bodies with DND1 in *Nanos2 KO* germ cells *in vivo* (Suzuki et al., 2012). Furthermore, the N-terminal is also relatively similar in amino acid sequence (Fig. 6A). Therefore, I hypothesized that these NANOS3 domains themselves are able to replace the respective NANOS2 domains. For this purpose, I created two chimeric proteins with either the NANOS2 or 3 ZF and full N-terminal (Fig. 6B). As NANOS3 has a longer C-terminal than NANOS2, this extra C-terminal sequence was deleted to examine whether it interferes with DND1 binding. As described in Methods, chimera mice expressing each chimeric protein were created via an ES-mediated strategy (Shimada et al., 2019) with the help of the mouse unit and the resulting chimeric germ cells were analyzed for *Nanos2 KO* phenotypes from E15.5.

Both 3xF-NANOS2-N58-NANOS3-ZF(Δ C46) and 3xF-NANOS3-N54-NANOS2-ZF chimeric proteins were expressed, and had a similar cytoplasmic localization pattern to endogenous NANOS2 (Fig. 6C). However, although neither mutant fully rescued the male differentiation pathway, as demonstrated by the lack of/weak DNMT3L expression, the quantification data suggest slight rescue via the 3xF-NANOS3-N54-NANOS2-ZF chimeric protein (Fig. 6D, E). The majority of wild-type (FLAG-negative) germ cells in the same testis had high DNMT3L expression. At E15.5, 3xF-NANOS2-N58-NANOS3-ZF(Δ C46)-expressing cells also expressed STRA8, which is normally absent but becomes upregulated in *Nanos2*-null germ cells. However, there was a delay in the upregulation of STRA8 in 3xF-NANOS3-N54-NANOS2-ZF-expressing cells. Most mutant cells were negative for STRA8 at E15.5, but by E17.5, STRA8 was upregulated (Fig. 6F), again suggesting slight rescue by the 3xF-NANOS3-N54-NANOS2-ZF chimeric protein. This means that the NANOS2 ZF plays a more important role in RNA regulation of certain targets than the NANOS2 N-terminal. However, endogenous NANOS3 was still upregulated in all mutant germ cells according to immunostaining (Fig. 7A) because our NANOS3 antibody detects the C-terminal of NANOS3, thus only endogenous NANOS3 is detected in chimeric germ cells (Fig. 7B). Moreover, the NANOS2 target *Dazl* was not repressed in chimeric germ cells based on the increased DAZL protein expression (Fig. 7C, D).

The DND1 protein level is dependent on strong binding with the NANOS2 ZF domain

We found that both chimeric NANOS proteins failed to replace endogenous NANOS2 function. To investigate the reason, I further examined the properties of germ cells expressing chimeric proteins. Wild-type NANOS2 interacts with DND1 and localizes to P-bodies in male germ cells (Suzuki et al., 2016). I observed that DND1 was similarly localized to foci with both chimeric proteins (Fig. 8A). To assess the formation of P-bodies, I stained with an antibody against Rck/p54 (DDX6), a known P-body component

that represses translation (Chu and Rana, 2006; Shimada et al., 2019). Chimeric germ cells expressing either 3xF-NANOS2-N58-NANOS3-ZF(Δ C46) or 3xF-NANOS3-N54-NANOS2-ZF had DDX6 foci, suggesting the formation of P-bodies (Fig. 8A,B,C). However, the DND1 protein level was reduced, especially in 3xF-NANOS2-N58-NANOS3-ZF(Δ C46)-expressing cells (Fig. 8A,B, Fig. 9A), similar to the reduction observed in *Nanos2* KO and dKO embryos. This suggests that the DND1 protein level is dependent on the presence of the NANOS2 ZF because the *Dnd1* mRNA level does not change in *Nanos2* KO (Fig. 4C). As there was limited DND1-chimeric protein localization, I considered that the binding of the proteins was affected.

To assess this possibility, I conducted several biochemical analyses. Using HEK293T cells, HA-DND1 was transfected with FLAG-tagged NANOS2 or NANOS3 to evaluate the binding strength *in vitro*. The amount of DND1 precipitated with NANOS3 was much lower than that for NANOS2, demonstrating the weaker binding strength of DND1 with the NANOS3 ZF (Fig. 9B). Next, the binding strength of the chimeric proteins with DND1 was assessed. 3xF-NANOS3-N54-NANOS2-ZF precipitated DND1 to the same degree as NANOS2 and addition of the NANOS3 C-terminal had no effect on DND1 binding (Fig. 9B). However, 3xF-NANOS2-N58-NANOS3-ZF(Δ C46) was poorly expressed, suggesting that the NANOS3 C-terminal is needed for protein stabilization *in vitro* (Fig. 9B). As 3xF-NANOS2-N58-NANOS3-ZF(Δ C46) was expressed at levels similar to endogenous NANOS2 *in vivo* (Fig. 6C), other germ-cell specific factors may be involved in the stabilization of NANOS3 protein *in vivo*. Addition of the NANOS3 C-terminal restored 3xF-NANOS2-N58-NANOS3-ZF(Δ C46) expression in HEK293T cells (Fig. 9B), but it was still unable to precipitate more DND1. Thus, the NANOS2 ZF itself was reconfirmed as key for DND1 binding.

Specific NANOS2 amino acid configuration is required to carry out its activity

The chimeric protein expression analyses demonstrated that the ZF domain is responsible for the difference in binding ability of NANOS proteins to DND1. However, the T-Coffee algorithm Expresso (Armougom et al., 2006; Di Tommaso et al., 2011; Notredame et al., 2000; O et al., 2004; Poirot et al., 2004), which aligns protein sequences based on protein structural information, indicated that the NANOS2 and 3 ZF amino acid sequences are markedly similar. It was previously reported that mutation of C61 and C96 to alanine in the CCHC-CCHC ZF motif of NANOS2 abolished DND1 interaction (Suzuki et al., 2016). Therefore, I examined if the amino acids flanking the CCHC repeats that are different between NANOS2 and NANOS3 can explain the difference in DND1 binding strength. Point mutations were introduced to change the NANOS2 amino acid to the respective NANOS3 amino acid: I60L, N62S, Q78V, V87L, L98Q and Y111F (Fig. 10A). On immunoprecipitation with point mutants and DND1, all NANOS2 mutants had lower binding strength with DND1, with NANOS2-Y111F being the most reduced (Fig. 10B). As a single mutation was able to weaken NANOS2-DND1 binding, the opposite experiment was carried out and NANOS3 was mutated at L56I, S58N and F107Y, which equate to NANOS2 I60L, N62S and Y111F, respectively. The single mutation of F107Y was able to slightly increase the binding strength of NANOS3 for DND1, but all three mutations and even all six mutations together failed to further increase the amount of DND1 precipitated (Fig. 10C). Thus, although position Y111 may be important for DND1 binding, the entire NANOS2 ZF amino acid sequence is needed for correct DND1 interaction and RNA regulation. Using Phyre2 to create 3D models of the ZF domain (Kelley et al., 2015), I examined the differences between NANOS2 and NANOS3 (NANOS2 protein sequence: MGI: 2676627; NANOS3 protein sequence: MGI: 2675387) (Fig. 10D). There was a slight difference in the side chain position between NANOS2 Y111 and NANOS3 F107 in relation to the CCHC side chains, which may affect binding.

The reduced binding between DND1 and the NANOS3 ZF explains why 3xNANOS2-N58-

NANOS3-ZF(Δ C46) was unable to rescue male-type differentiation, but 3xF-NANOS3-N54-NANOS2-ZF had no decrease in binding strength and failed to rescue male-type differentiation as well. The NANOS2 N-terminal binds to the CNOT1 component of the CCR4-NOT complex in vitro, and previous studies revealed that full-length mouse NANOS3 is unable to directly bind CNOT1 (Suzuki et al., 2014, 2012). However, a previous study reported a CNOT interaction motif (NIM) containing conserved three amino acid residues (FWY) in the N-terminal of NANOS in several species (Bhandari et al., 2014). Human, *Xenopus* and zebrafish NANOS3 NIMs were able to directly bind CNOT1 (Bhandari et al., 2014). As mouse (m)NANOS3 also has this conserved NIM (Fig. 11A), I conducted a GST-pull-down experiment using both MBP-fused full-length mNANOS3 and NANOS3 NIMs to compare their ability to bind CNOT1. As previously reported (Suzuki et al., 2014), full-length mNANOS3 cannot bind CNOT1, but both full-length mNANOS2 and the human (hu)NANOS3 NIM can (Fig. 11B). However, mNANOS3-NIM, despite being different from huNANOS3-NIM by only three amino acids (Fig. 11C), was unable to strongly bind CNOT1 when compared with huNANOS3-NIM. To examine this further, I made a mutant mNANOS3 NIM changing the second amino acid position from N to D, making it the same amino acid as in huNANOS3 and mNANOS2 NIMs. This mutant mNANOS3 NIM was still unable to bind CNOT1 strongly (Fig. 11C). Therefore, there is some other factor or modification involved.

The lack of rescue by 3xF-NANOS3-N54-NANOS2-ZF can be attributed to a reduced ability to bind CNOT1. This result is consistent with a previous study in which NANOS2 lacking the N-terminal failed to rescue *Nanos2*-null germ cells (Suzuki et al., 2012).

1.4 Discussion

The long-standing question of why the structurally related NANOS proteins exhibit unequal functional redundancy during germ cell development was partly answered by my genetic and biochemical studies.

There were two major questions: 1) Why is NANOS3 unable to rescue NANOS2 function even though its expression is strongly up-regulated in the absence of NANOS2, and 2) is there any rescue event via the up-regulated NANOS3. As shown in Fig. 3A, conditional double knockout of *Nanos2* and 3 led to the rapid loss of germ cells, demonstrating that NANOS3 functions in the absence of NANOS2 to protect germ cells from apoptotic cell death. On the other hand, conditional deletion of NANOS3 in the presence of NANOS2 did not cause any phenotype other than increased DAZL expression, but this increase had no effect on male differentiation. Thus, NANOS2 alone can protect against germ cell death and promote the male differentiation program.

The combination of the different NANOS2 functional domains, N-terminal and ZF, is likely what enables full protein functionality and progression of male germ cell differentiation. As the NANOS3 and NANOS2 ZF domains have a similar structure, they were hypothesized to be able to replace each other. However, this was not the case and the NANOS3 ZF only weakly bound DND1, as shown in Fig. 9B. To analyze the reason for this weaker binding, point-mutation experiments were carried out, demonstrating that sequence specificity plays a large role in the binding of DND1. Binding strength was reduced the most by mutations next to the last cysteines (I60L, N62S, and Y111F) of the CCHC repeats in the NANOS2 ZF domain. These cysteines may create a binding area for DND1, and the surrounding amino acids may need to be in a specific conformation to accommodate tight protein-protein/RNA interaction. As shown in Fig. 10B, NANOS2-Y111F had the greatest reduction in binding strength, which may have been caused by the small change in amino acid side chain from tyrosine to phenylalanine. Using Phyre2 to create 3D models of the ZF domain, I examined differences between NANOS2 and 3. Mutation of NANOS2 Y111 to F111 caused the amino acid side chain orientation to shift to that observed in the NANOS3 model. Although it is currently unknown how and where DND1 binds, as mutation of Y111 had strong negative effects, it may be involved in DND1 binding. Phosphorylation of tyrosine residues has

been reported to affect protein binding and frequently occurs on binding interfaces, stabilizing protein complexes (Nishi et al., 2011). One of the RNA recognition motifs of human DND1 was recently crystallized (Kumari and Bhavesh, 2020), but how the NANOS2 ZF and mouse DND1 bind with mRNA remains undetermined.

The mechanism of how NANOS2 RNA targets are selected remains unknown. Currently, the only known mRNA target regulated during male-type differentiation is *Dazl* (Kato et al., 2016). Both chimeric mutants were likely unable to properly target and regulate RNA due to different reasons; the low DND1 binding strength (3xF-Nanos2N58-Nanos3ZF(Δ C46)) and inability to bind to the CCR4-NOT deadenylation complex correctly (3xF-Nanos3N54-Nanos2ZF). In the case of 3xF-Nanos3N54-Nanos2ZF germ cells, the phenotype was milder than that of 3xF-Nanos2N58-Nanos3ZF(Δ C46) germ cells in that DND1 expression was maintained (Fig. 8A), more cells expressed DNMT3L and STRA8 upregulation was delayed (Fig. 6D,E,F), probably due to the presence of the NANOS2 ZF. However, DND1 binding with the NANOS2 ZF alone is insufficient for the male pathway to proceed. The presence of DDX6 foci colocalized with DND1 signal, representing P-bodies, suggested that RNA was bound, but whether these P-bodies are similar to those formed in wild-type germ cells remains unknown. Therefore, even if RNAs were correctly targeted, P-body components, such as CCR4-NOT, may not be functioning correctly, as suggested by the increased protein expression of DAZL (Fig. 7C), whose mRNA is targeted by NANOS2. This may have been because the mNANOS3 NIM cannot strongly bind CNOT1. The mNANOS3 NIM may be affected by other factors or folds to take a different protein structure, which thereby blocks its direct binding with CNOT1. It has been reported that mouse NANOS3 can directly bind CNOT8 *in vitro*, which may explain the inability to initiate male differentiation. CNOT1 is a scaffold protein and is able to interact with the deadenylases CNOT6, 6L, 7 and 8. On the other hand, CNOT8 competes with CNOT7 for binding to CNOT1, resulting in lower deadenylase activity (Suzuki et al., 2014).

There may also be another factor that mediates NANOS3-CNOT-DND1 *in vivo*, but DND1 is not considered a partner protein of NANOS3. In cultured cells, NANOS3 does not localize with DND1 in P-bodies, but in *Nanos2* KO germ cells it does (Fig. 12A,B) Thus, protein interactions *in vivo* are different from in cultured cells and may be species-specific. For example, 3xF-NANOS2-N58-NANOS3-ZF(Δ C46) was normally expressed in chimeric mouse germ cells but was hardly expressed in HEK293T cells, suggesting that something is binding and/or stabilizing it *in vivo*. The *in vivo* functions of human NANOS3 are largely unknown, and this study suggests that they vary from those of mouse NANOS3.

Based on my study, the role of NANOS3 is to protect against cell death even after the germ cells enter the gonad. The sudden loss of germ cells between E13.5 and 14.5 observed in the dKO indicates the presence of a checkpoint for germ cell viability. In wild-type embryos, this timing is when there is a shift in the balance of NANOS2 and 3 expression, as well as events marking sex differentiation; female germ cells enter meiosis, whereas male germ cells arrest the cell cycle. There is a wave of apoptosis among PGCs at E13.5 (Coucovanis et al., 1993). As NANOS3 mRNA expression stops after E13.5 in female germ cells, their successful meiotic entry may protect them from continued apoptosis. On the other hand, male germ cells begin to express NANOS2, which is known to regulate the cell cycle. *Nanos2* expression and male differentiation were reported to mark an apoptosis-resistant state of germ cells, whereas the undifferentiated state was more prone to apoptosis (Nguyen and Laird, 2019). *Nanos2* KO male germ cells may not immediately die because NANOS3 is upregulated and they enter an abnormal cell cycle with STRA8 induction. As reported waves of apoptosis are observed before meiotic entry in both males and females (Coucovanis et al., 1993; Rucker et al., 2000), and the dKO germ cells expressed Ki-67, indicating failure of cell cycle arrest, the loss of germ cells in the dKO mice after E13.5 may have resulted from their inability to clear a cell cycle checkpoint and avoid apoptosis. The presence of either NANOS protein enables male germ cells to clear this hypothetical checkpoint, but only NANOS2 can promote the

subsequent male pathway. The apparent superiority of NANOS2 likely resides in its structural properties, i.e., binding ability to CNOT1 and DND1, which is defective in NANOS3.

I speculate that NANOS3 cannot properly regulate NANOS2 targets, but it is still possible that it binds and regulates other mRNAs, such as those related to apoptosis (Suzuki et al., 2008), in the absence of NANOS2. Furthermore, NANOS3 expression may be related to the temporary cell cycle arrest and STRA8 upregulation observed in *Nanos2* KO at E14.5 because these phenotypes were not observed in the dKO. Determining how mRNA are successfully selected and regulated by RBPs will further the current understanding of how the male pathway is initiated. In conclusion, my study sheds light on the functional differences between NANOS2 and NANOS3 in germ cell development, providing an example of how two homologous proteins can have varying functions despite their similar structure.

Chapter 2

2.1 Background

As described in Chapter 1, NANOS2 is an evolutionarily conserved RBP involved in germ cell development that functions by binding with a partner protein, DND1, leading to male germ cell differentiation. Functional P-bodies, granules for RNA storage and degradation formed through phase separation, are needed for the male pathway to proceed in male germ cells. However, the individual roles of NANOS2 and DND1 in this process of RNA targeting to P-bodies remain unclear.

Currently, no crystal structure is available for mouse DND1, and although I and others tried several methods to purify recombinant DND1 to solve its structure, they were unsuccessful because DND1 is highly insoluble. As such biochemical methods failed, a different method is needed to reveal how DND1 and NANOS2 interact and bind mRNA. In addition, how the mRNA targets are selected and what happens to them inside P-bodies are unanswered questions. Therefore, I decided to use live imaging techniques to examine the interactions among DND1, NANOS2, and mRNA, and the subsequent formation of P-bodies. For this purpose, I employed a dCas13 system (Abudayyeh et al., 2017, 2016). dCas13 is an endonuclease-dead RNA-specific RNase. Using the EGFP-fused dCas13 and a specific guide RNA, germ cell-specific mRNA can be visualized upon transfection in cultured cells. I used mouse NIH3T3 cells that express NANOS2 and DND1, which can reproduce the NANOS2-DND1

cascade in order to observe the dynamics of P-body components and NANOS2-target mRNA *Dazl* (Suzuki et al., 2016, Kato et al., 2016). In addition, I employed fluorescently labelled proteins to visualize the formation of P-bodies and the interactions of RBPs. The purpose of this study was to clarify how NANOS2 and DND1 contribute to target-RNA binding and the formation of P-bodies.

2.2 Materials and Methods

Cell culture

HEK-293T, NIH3T3 and ciN2D13T3 cells were cultured in DMEM supplemented with 10% FBS, L-glutamine and penicillin/streptomycin at 37°C in 5% CO₂.

Western Blotting

CiN2D13T3 cells were lysed in lysis buffer. After centrifugation, supernatants were boiled in 2x sample buffer for 5 min and run on gels for sodium dodecyl sulfate-polyacrylamide gel electrophoresis (SDS-PAGE). They were then transferred to PVDF (Immobilon) membranes. Membranes were blocked in 5% skim milk/ PBST for 1 hr at RT. They were then incubated with the following primary antibodies overnight at 4°C: anti-DAZL, anti-HA and anti-FLAG-HRP. After washing 3 times with PBST, membranes were incubated with HRP-conjugated secondary antibodies for 1 hr at RT. Protein bands were visualized using SuperSignalTM West Femto Maximum Sensitivity Substrate (Thermo Scientific).

mRNA imaging using dCas13

dLwaCas13a–NF and the Cas13 guide expression vector were purchased from Addgene. The targeting guide for *ACTB* was created following the report by Abudayyeh et al. As *dazl* is germ cell-specific, *Dazl* with its 3'UTR was cloned into the pcDNA3.1 expression vector and used to assess guide specificity.

Several targeting guides for *Dazl* were created following the same procedure as for the *ACTB* guide. To image *ACTB*, HEK-293T cells were transfected with dLwaCas13a–NF, the *ACTB* guide and DDX6-mcherry constructs using PEI. Forty-eight hours after transfection, stress granule formation was induced by culturing the cells in medium with 400 μ M sodium arsenite for 1 hour and imaged using a 100x lens at 37°C in 5% CO₂ with the FV1200 confocal microscope. To image *Dazl*, NIH3T3 cells were transfected with dLwaCas13a–NF and a *Dazl* guide with or without the *Dazl*-3'UTR construct using Lipofectamine LTX + Plus. Forty-eight hours after transfection, cells were imaged using a 100x lens at 37°C in 5% CO₂ with the FV1200 confocal microscope. Z-stack images were compiled to create 3D time-lapse animations using the included software.

Fluorescence live imaging

For 4-color live imaging, BFP2, tagRFP and mi670 fluorescent proteins were used. tagRFP and mi670 were gifts from Dr. Wada at Fukushima Medical University. BFP2 was added to the N-terminal of NANOS2 and del-N-NANOS2. tagRFP was added to the C-terminal of DND1, DND1R98A and DDX6. mi670 was added to the C-terminal of DCP1a and DDX6. All constructs were created using the InFusion system and inserted into the pcDNA3.1 expression vector. NIH3T3 cells were transfected with constructs for the dCas13 system and a combination of BFP2-, tag-RFP- and mi670-tagged proteins using lipofectamine LTX + Plus. Live imaging was performed 24-48 hours after transfection on either the Olympus FV1200 confocal microscope or Deltavision Ultra.

Immunostaining and RNA visualization by ViewRNA

After removing the culture medium, cells were fixed with 4% paraformaldehyde/PBS for 15 min at RT. They were then permeabilized with 0.3% Triton-100 for 15 min at RT. Cells were blocked with 3% skim

milk/PBST for 30 min and then incubated overnight with the following primary antibodies: mouse anti-NANOS2, mouse anti-CNOT1, rat anti-HA, rabbit-anti-Rck and chicken anti-GFP. After washing with PBST, cells were incubated with secondary antibodies conjugated with Alexa Fluor 405, 488, 594 and 647 for 30 min at RT. DNA was stained with DAPI. For ViewRNA staining of *Dazl* mRNA, the ViewRNA Cell Plus kit was used following the manufacturer's instructions with the *Dazl* probe set. P-bodies were stained using anti-Rck. For ViewRNA and immunostaining, cells were imaged using Olympus FV1200 confocal microscope. Super-resolution microscopy was performed using the Olympus IXplore SpinSR microscope.

Statistical Analysis

For the colocalization analysis, Coloc (a package for colocalisation analyses, <https://cran.r-project.org/web/packages/coloc/vignettes/vignette.html>) was applied to Z-stack images of cells. The presented correlation coefficients are the r-values after Costes thresholding. The cytofluorograms are a scatterplot of the spatial localization and intensity of pixels in 2 channels. The diagonal line in the middle of the plot is the intensity ratio.

2.3 Results

Evaluation of the dCas13 system for live imaging of mRNA

As one of my key questions was the mechanism by which NANOS2 binds and recruits RNA to P-bodies, I need a new method to visualize RNA and proteins together in P-bodies. In 2017, Abudayyeh et al. reported a method to visualize RNA in cells using GFP-fused catalytically inactive Cas13, which specifically binds RNA (Abudayyeh et al., 2016; 2017). RNA imaging with Cas13 is a relatively new technique with a reportedly high specificity, but there are several problems that must be overcome to use

it. The first is that Cas13 functions similarly to Cas9, requiring a guide, but several guides need to be tested for the desired target RNA. Another problem is that NANOS2 and DND1 are germ cell-specific proteins, and must be exogenously expressed to observe P-body formation in cells. As embryonic germ cells are few in number and weak under cultured conditions, a cultured cell system to evaluate the dCas13 imaging system is required.

To assess the feasibility of this system, I first observed the movement of human beta-actin (*ACTB*) mRNA into stress granules, which are another type of RNP granule that store transcripts under stress conditions (Kedersha et al., 2005; Buchan et al., 2009). HEK-293T cells were transfected with dCas13, *ACTB* guide and DDX6-mcherry constructs referring to the method reported by Abudayyeh et al. (Fig. 13A). After culturing the cells with arsenite to induce stress, I visualized mRNA localization to stress granules. As negative controls, cells transfected without a guide and with a non-targeting guide were imaged. This dCas13 construct inhibits its own transcription when not bound to a target, therefore, without a guide, only nuclear expression or no GFP expression is observed (Fig. 13B, middle). On the other hand, with the *ACTB* guide, the GFP signals representing *ACTB* mRNA made pools within the cytoplasm, and DDX6-mcherry-positive stress granules formed around these pools (Fig. 13B, right). When cells were not transfected with the guide, these beta-actin RNA pools were not observed. These results were similar to those reported in the original paper, confirming that this system works well.

Next, I moved to applying this system to a specific NANOS2-target mRNA, *Dazl*. As it was previously reported that NANOS2 binds the *Dazl* 3'UTR (Kato et al., 2016), I designed several guides in the N-terminal region to avoid Cas13 interference. *Dazl* is also germ cell specific, which made guide assessment simpler. In order to test their specificity, NIH3T3 cells were transfected with each guide with or without *Dazl*. As shown in Fig. 13C, guide 1 resulted in GFP signal both with and without *Dazl*, indicating that other mRNA were targeted. Guide #2 resulted in GFP signal only when *Dazl* was present

with limited background, as shown in Fig. 13D. I judged the specificity of guide #2 to be sufficiently high for detection and decided to employ this guide in all experiments thereafter.

NANOS2 and DND1 alter Dazl localization

The current hypothesis for the mechanism of mRNA regulation by NANOS2 is that upon its expression, it binds DND1 and targets specific mRNA, and the complex moves to P-bodies to be possibly degraded. To confirm this process, I therefore first performed time lapse imaging of *Dazl* localization before and after the induction of NANOS2 and DND1. NIH3T3 cells that express NANOS2 and DND1 upon doxycycline (Dox) addition (ciN2D1-3T3) were created here in our lab by Dr. Hirano (Fig. 14A). These cells are able to reproduce the repression of DAZL by NANOS2 and DND1 (Fig. 14B). Using these cells, I transfected dCas13, guide #2 and *Dazl*+3'UTR constructs to observe mRNA localization to P-bodies, as shown in Fig 14C. One day after transfection, I added Dox and began imaging. In control cells without Dox, there were a few P-bodies, with most *Dazl* localized to the cytoplasm and somewhat in P-bodies (Fig. 14D). This was expected considering the functions of P-bodies as storage granules. Once Dox was added, the number of P-bodies increased along with the increasing amount of *Dazl* based on the strong GFP accumulation in and around P-body foci. By 6 hours after doxycycline addition, both NANOS2 and DND1 are expressed and large P-bodies with a characteristic *Dazl* localization pattern were observed. Most *Dazl* had accumulated around P-bodies, suggesting that it was being actively targeted by NANOS2 and DND1 (Fig. 14D).

For further confirmation of *Dazl* targeting to P-bodies, I employed the ViewRNA system to stain *Dazl* mRNA in ciN2D13T3 cells. Similar to the live imaging results, without NANOS2 and DND1, most *Dazl* was in the cytoplasm and not colocalized with DDX6 ($r=0.21$) (Fig. 14E, F, G). After adding Dox, the localization pattern shifted, and more *Dazl* was localized to P-bodies, with a colocalization

coefficient of $r = 0.52$ (Fig. 14E, F, G). Based on these results, *Dazl* is targeted to P-bodies when NANOS2 and DND1 are expressed, which was expected.

DND1 binds Dazl, but NANOS2 does not

Based on the live imaging experiments, *Dazl* is actively recruited to P-bodies when NANOS2 and DND1 are present. However, the major question is which RBP is actually binding *Dazl*: NANOS2 or DND1. Using super resolution microscopy of immunostained cells, NANOS2, DND1 and *Dazl* exhibit a stacking pattern in P-bodies consistent with the condensation of phase separation (Fig. 15A), making it unclear what is associated with what at a given time point. Thus to address the above question, live imaging of the individual proteins involved is necessary. I took advantage of the variety of fluorescent proteins currently available and created a 4-color protein set, namely BFP2-tagged NANOS2, tagRFP-tagged DND1 and mi670-tagged DCP1a, with *Dazl* mRNA being marked by GFP-tagged dCas13 (Fig. 15B). Using this combination to represent the condition in germ cells, I performed 4-color live imaging. Consistent with what has been reported *in vivo* in germ cells, NANOS2, DND1 and *Dazl* all colocalized within DCP1a foci (Fig. 15C). However, in the cytoplasm, DND1 alone colocalized with *Dazl* was observed, but unexpectedly, NANOS2 alone was not colocalized with *Dazl*. This suggested that DND1 was actually binding the target RNA. In support of this idea, on live imaging, DND1 was observed directly interacting with *Dazl*, whereas NANOS2 interacted with DND1 (Fig. 15D).

To further investigate the roles of these proteins, cells that express only DND1 or NANOS2 were imaged. In the case of cells expressing only NANOS2, *Dazl* was spread throughout the cytoplasm, with no clear localization to P-bodies or colocalization with NANOS2 (Fig. 16A). On the other hand, in cells expressing only DND1, there was a greater amount of *Dazl* was colocalized with DND1 but few of these accumulations were localized to large DCP1a foci (Fig. 16B), suggesting that although more RNA was

possibly bound, it was unable to be specifically targeted to P-bodies. Without NANOS2, bound *Dazl* was not well recruited to P-bodies, whereas, without DND1, NANOS2-target mRNA mostly remained in the cytoplasm with only slight overlap with DCP1a. In both cases, there were no large DCP1a foci, reflecting poor mRNA recruitment and poor P-body assembly.

To confirm the role of DND1 as an RNA-recruiter, I used a recently reported DND1 mutant, DND1R98A, which has weakened RNA-binding ability (Duszczuk et al., 2019). In the presence of wild-type DND1 (Fig. 17A), large P-bodies were formed and they remained stable over time. DND1 and *Dazl* were also colocalized with NANOS2 (Fig. 17A,B). However, in the presence of DND1R98A with NANOS2, the DCP1a foci size was small, and over time, the small P-bodies that were formed dissipated (Fig. 17C, yellow arrowheads). In addition, the amount of *Dazl* colocalized with DND1R98A decreased (Fig. 17C, D). This was in contrast to the DND1-only case in which a large amount of DND1 and *Dazl* accumulated together (Fig. 10B), confirming that DND1, not NANOS2, is required to strongly bind target mRNA. Moreover, even though DND1R98A and NANOS2 colocalized (Fig. 17D), without strong binding of mRNA, stable P-bodies were not formed.

Lastly, I used a zinc finger mutant of NANOS2 (NANOS2-ZM) to examine the case when DND1 is not bound by NANOS2. Suzuki et al. previously reported that this mutant cannot bind DND1 and no P-bodies are assembled in germ cells expressing NANOS2-ZM (Suzuki et al., 2014, 2016). However, when transfected into NIH3T3 cells, NANOS2-ZM aggregated with all DND1 and *Dazl* (Fig. 17E, F). As this protein no longer has its zinc finger structure, this aggregation of protein and mRNA is likely an artifact due to the non-functional NANOS2.

Based on live imaging of wild-type and mutant proteins, DND1, not NANOS2, binds *Dazl*, and when an insufficient amount of mRNA is bound, P-bodies are not formed. As such, DND1 can strongly bind RNA, but NANOS2 likely regulates which mRNA is bound and their subsequent localization.

NANOS2 controls P-body localization through binding CNOT1

According to live imaging using the individual proteins and mutant DND1, I found that even though *Dazl* is a NANOS2 target, it is likely bound by DND1. However, DND1-bound *Dazl* was not localized to P-bodies unless NANOS2 was also present. As NANOS2 also binds CNOT1, a component of the CCR4-NOT deadenylation complex that is important for P-body formation (Ito et al., 2011), I hypothesized that the recruitment of CNOT1 by NANOS2 is what enables the localization of target mRNA to P-bodies. NANOS2 has a CNOT1 binding motif in its N-terminal, and if this N-terminal is deleted, CNOT1 cannot be bound, and mice carrying such mutant NANOS2 were sterile (Suzuki et al., 2012). I thus used BFP2-tagged NANOS2 lacking the N-terminal (del-N-NANOS2) to evaluate *Dazl* localization when CNOT1 is not recruited. In the wild-type case, DND1 and NANOS2 colocalized with *Dazl* (Fig. 18A, top). However, in the del-N-NANOS2 case, most mutant NANOS2 was alone in the cytoplasm, with limited colocalization with *Dazl* and DND1 (Fig. 18A, B, C, bottom). When stained with anti-CNOT1, there were no large CNOT1 foci, which are usually observed in the wild-type case (Fig. 18A, top). Furthermore, rather than these proteins being localized inside DCP1a foci (Fig. 12B top), they were located outside (Fig. 18B, bottom). However, DND1 was colocalized with DDX6 and bound a limited amount of *Dazl* (Fig. 18C, bottom). However, when DND1 alone was expressed, a large amount of *Dazl* was targeted (Fig. 16B). This suggests that if NANOS2 is present and cannot bind CNOT1, DND1 binding and the mechanism by which target mRNA are targeted is disrupted. Therefore, the recruitment of CNOT1 by NANOS2 may regulate DND1-mRNA binding and the subsequent formation of P-bodies through NANOS2-DND1-mRNA complexes.

2.4 Discussion

Live imaging to support a model of P-body formation

The formation of P-bodies in germ cells by NANOS2 and DND1 plays an essential role in the progression of male germ cell differentiation. However, until now, no study has investigated the individual roles of these proteins or their effects on mRNA via live imaging. Being RBPs, the lack of a system to easily visualize RNA has made their functional analysis difficult. As the purpose of this study was to differentiate the individual roles of NANOS2 and DND1 during this process of mRNA regulation through the formation of P-bodies, I devised a method to visualize RNA in real time alongside the individual proteins. Based on my time-lapse imaging, I propose the following model of the events leading to mRNA regulation by NANOS2 and DND1: Upon the expression of NANOS2, DND1 is regulated to bind a specific target, in this case *Dazl*. NANOS2 then binds *Dazl*-bound DND1, bringing with it CNOT1.

Why does Dazl accumulate around P-bodies?

The increased amount of *Dazl* in and around P-bodies after the induction of NANOS2 and DND1 expression (Fig. 14D, left) was an expected result considering that *Dazl* is a NANOS2 target that is regulated through P-bodies (Kato et al., 2016, Shimada et al., 2019). However, NANOS2 alone cannot associate with *Dazl* (Suzuki et al., 2016), leading to the question of which RBP is actually binding. Indeed, according to my live imaging, NANOS2 is not the protein that first binds *Dazl*. In cells expressing NANOS2, DND1 and *Dazl*, NANOS2 and *Dazl* were not colocalized alone in the cytoplasm outside of P-bodies. As an initial step towards P-body formation, RBPs come together to form a scaffold (Buchan et al., 2014). The P-body marker DCP1a only colocalized with the complex of NANOS2, DND1 and bound *Dazl* (Fig. 15C). This is consistent with non-translating mRNA and decapping proteins, such as DCP1a, being necessary for P-bodies to form (Sheth, 2003, Eulalio et al., 2007, Aizer et al., 2008, Buchan et al., 2014). However, I found that NANOS2 alone has limited affinity even for its

target mRNA.

On the contrary, DND1 was commonly localized with *Dazl*, reflecting its high affinity for mRNA. The presence of two RNA recognition motifs in DND1 may increase its binding affinity, but they are not considered to recognize specific sequences other than U-rich domains (Corley et al., 2020, Gross-Thebing and Raz, 2020). DND1 alone was unable to induce the formation of large round P-bodies even though a large amount colocalized with *Dazl* (Fig. 16B). It was previously reported that if there is a surplus of decay enzymes compared with the amount of non-translating mRNA, mRNA can be degraded quickly without P-bodies being observed (Franks and Lykke-Andersen, 2008). As DND1 itself is known to regulate mRNA (Gross-Thebing and Raz, 2020), the lack of large P-bodies may have been because *Dazl* was quickly degraded. However, as *Dazl* is not a DND1 target, it is also possible that the observed colocalization was random binding and *Dazl* was quickly released thereafter.

On the other hand, as *Dazl* continued to accumulate around P-bodies over time in the presence of NANOS2, DND1 may instead only act as an RNA recruiter, whereas NANOS2 functions as a regulator. It is therefore possible that *Dazl* is accumulated and stored in P-bodies rather than being immediately degraded, consistent with the role of NANOS2 as a translational repressor and P-bodies as sites of both decay and storage (Suzuki et al., 2007, Aizer et al., 2014, Bhandari et al., 2014, Zhou et al., 2015).

Roles of NANOS2 and DND1 in P-body formation

The first step in eukaryotic P-body formation is the repression of translation, with DDX6 binding the mRNA (Ayache et al., 2015, Franks and Lykke-Andersen, 2008). Next, P-body components, such as CNOT1 and DCP1a, are recruited, leading to the formation of a scaffold with RBPs (Franks and Lykke-Andersen, 2008, Buchan, 2014). With DND1R98A, which has weaker mRNA binding ability, there were fewer stable P-bodies (Fig. 17B), demonstrating not only the necessity of bound repressed mRNA for the maintenance of P-bodies, but also the role of DND1 as the major mRNA binder.

NANOS2 binds CNOT1 via the interacting motif in its N-terminal (Suzuki et al., 2012, Bhandari et al., 2014); therefore, deletion of this motif will prevent CNOT1 binding and affect P-body assembly. CNOT1 helps to stabilize the other CCR4-NOT enzymatic subunits for deadenylase activity (Ito et al., 2011, Shirai et al., 2014). Although the overall cytoplasmic localization pattern of del-N-NANOS2 was not different from wild-type NANOS2, the protein was not colocalized well with DND1. (Fig. 18A,B,C, bottom). In addition, DND1 was no longer binding *Dazl* (Fig. A, C, bottom). This suggests that without the ability to form mRNA-regulatory complexes through CNOT1 and create stable P-bodies, NANOS2 and DND1 dissociate and DND1 releases *Dazl* because it is no longer targeted. In the presence of Del-N-NANOS2, DND1 was instead located throughout the cytoplasm together with DDX6, likely binding mRNAs other than *Dazl*. It was previously reported that human DDX6 and CNOT1 bind, and then indirectly interact with DCP1 and 2, providing a link between repression and decapping (Chen et al., 2014). As no complete colocalization of Del-N-NANOS2, DND1, DDX6, and DCP1a was observed, the loss of direct NANOS2-CNOT1 binding affects the formation of the P-body scaffold. Therefore, in the del-N-NANOS2 case, because CNOT1 was not recruited, P-bodies were unable to be maintained because of an unstable scaffold and mRNA regulation via NANOS2 was inhibited, thereby perturbing the interactions among the *Dazl*, DND1, and NANOS2.

DND1 and NANOS2 in the P-body scaffold

The control of DND1 by NANOS2 is also observed *in vivo* in germ cells, as the loss of the NANOS2 N-terminal leads to the loss of DND1 based on my results using chimeric mice (Wright et al., 2020). As such, NANOS2 and DND1 form a functional complex by having the strong RNA binding ability of DND1 with the P-body inducing properties of NANOS2. CNOT1 functions as a scaffold and its recruitment by NANOS2 likely promotes the formation of stable, long lasting P-bodies. Consistent with live imaging, the induction of NANOS2 and DND1 lead to the formation of many larger P-bodies

that contained *Dazl* mRNA inside. As proteins with RNA-binding domains play major roles in phase separation (Dodson and Kennedy, 2020), this accumulation of components likely reaches a threshold and induces phase separation for an energetically favorable configuration, and NANOS2, DND1, *Dazl* and all other P-body components form into spheres, with repressed *Dazl* continued to be brought for deadenylation.

Applicability of Cas13

Although it is relatively new, many techniques have been created using Cas13 to target specific RNA (Abudayyeh et al., 2016; 2017). Using the dCas13 system, the interactions of NANOS2 and DND1 with *Dazl* were able to be visualized in real time. Recent technological advances have made it possible to image RNA and proteins together. Although there are other systems, such as the MS2-MCP system, for imaging RNA, they each have disadvantages, especially regarding signal strength. The dCas13 system is not without drawbacks, such as the difficulty in guide creation and inability to track multiple targets, but it is expected to be improved, much like Cas9, and become a robust imaging modality in the future. By employing this novel system, I was able to distinguish the roles of two germ cell-specific proteins that function as a complex.

Thesis Conclusion

The development of healthy germ cells is vital to species maintenance, and the numerous proteins and mechanisms involved are major fields of study, especially towards a future of establishing a completely *in vitro* germ cell system. Recent technological advances have made it possible to examine the detailed interactions between RNA and proteins in cells, which are essential for their development. My thesis study focused on the functional redundancy of two germ cell-specific proteins, NANOS2 and 3, and the individual roles of NANOS2 and its partner in their RNA regulatory activity. Using conditional *Nanos3/Nanos2* knockout mice and chimeric mice expressing chimeric NANOS protein constructs, I was able to address a previously unanswered question of the function of NANOS3 in male germ cells. Single conditional knockout of *Nanos3* after colonization of the gonad caused no notable phenotype, but conditional double knockout of *Nanos2* and 3 led to the rapid loss of germ cells, suggesting that NANOS3 has a specific role in the absence of NANOS2 to continue to protect germ cells from apoptosis even though it cannot promote male germ cell differentiation. Furthermore, loss of DND1 protein was observed when the ZF of NANOS2 was replaced with that of NANOS3, demonstrating that DND1 and

NANOS2 binding is highly dependent on the specific NANOS2 structure itself. This dependency of DND1 expression on binding NANOS2 has not been reported previously. Using mutant proteins combined with the novel dCas13 system to visualize mRNA, I confirmed further that the specific structure of NANOS2 is required for its RNA regulatory ability through binding DND1 and CNOT1 to induce stable P-bodies. My live imaging system proposed a new model of how NANOS2 regulates RNA. This is important because such analyses will enable us to identify changes in the characteristics of RBPs when they are alone or in functional complexes. One overall message from my studies is that even if proteins are structurally similar, their functions can be altered by the associating factors.

Acknowledgements

I am deeply grateful to Professor Saga for her advice and guidance during my study. I also appreciate all of the comments and feedback from my progress committee members throughout. I would like to thank everyone in the Mammalian Development laboratory for their help and suggestions, and the mouse unit for helping make all of the mice I used. I also thank Dr. Suzuki at Yokohama National University for providing the constructs for the GST pulldown assay, and Dr. Wada at Fukushima Medical University for providing the tagRFP and mi670 constructs.

References

- Abudayyeh, O.O., Gootenberg, J.S., Essletzbichler, P., Han, S., Joung, J., Belanto, J.J., Verdine, V., Cox, D.B.T., Kellner, M.J., Regev, A., Lander, E.S., Voytas, D.F., Ting, A.Y., Zhang, F., 2017. RNA targeting with CRISPR–Cas13. *Nature* 550, 280–284. <https://doi.org/10.1038/nature24049>
- Abudayyeh, O.O., Gootenberg, J.S., Konermann, S., Joung, J., Slaymaker, I.M., Cox, D.B.T., Shmakov, S., Makarova, K.S., Semenova, E., Minakhin, L., Severinov, K., Regev, A., Lander, E.S., Koonin, E.V., Zhang, F., 2016. C2c2 is a single-component programmable RNA-guided RNA-targeting CRISPR effector. *Science* 353. <https://doi.org/10.1126/science.aaf5573>
- Aizer, A., Brody, Y., Ler, L.W., Sonenberg, N., Singer, R.H., Shav-Tal, Y., 2008. The Dynamics of Mammalian P Body Transport, Assembly, and Disassembly In Vivo. *MBoC* 19, 4154–4166. <https://doi.org/10.1091/mbc.e08-05-0513>
- Aizer, A., Kalo, A., Kafri, P., Shraga, A., Ben-Yishay, R., Jacob, A., Kinor, N., Shav-Tal, Y., 2014. Quantifying mRNA targeting to P-bodies in living human cells reveals their dual role in mRNA decay and storage. *J Cell Sci* 127, 4443–4456. <https://doi.org/10.1242/jcs.152975>
- Armougom, F., Moretti, S., Poirot, O., Audic, S., Dumas, P., Schaeli, B., Keduas, V., Notredame, C., 2006. Expresso: automatic incorporation of structural information in multiple sequence alignments using 3D-Coffee. *Nucleic Acids Res.* 34, W604-608. <https://doi.org/10.1093/nar/gkl092>
- Ayache, J., Bénard, M., Ernoult-Lange, M., Minshall, N., Standart, N., Kress, M., Weil, D., 2015. P-body assembly requires DDX6 repression complexes rather than decay or Ataxin2/2L complexes. *MBoC* 26, 2579–2595. <https://doi.org/10.1091/mbc.E15-03-0136>
- Bhandari, D., Raisch, T., Weichenrieder, O., Jonas, S., Izaurralde, E., 2014. Structural basis for the Nanos-mediated recruitment of the CCR4–NOT complex and translational repression. *Genes Dev.* 28, 888–901. <https://doi.org/10.1101/gad.237289.113>
- Buchan, J.R., 2014. mRNP granules: Assembly, function, and connections with disease. *RNA Biology* 11, 1019–1030. <https://doi.org/10.4161/15476286.2014.972208>
- Buchan, J.R., Parker, R., 2009. Eukaryotic stress granules: the ins and outs of translation. *Mol Cell* 36, 932–941. <https://doi.org/10.1016/j.molcel.2009.11.020>
- Butler, A., Hoffman, P., Smibert, P., Papalex, E., Satija, R., 2018. Integrating single-cell transcriptomic data across different conditions, technologies, and species. *Nature Biotechnology* 36, 411–420.

- <https://doi.org/10.1038/nbt.4096>
- Chen, Y., Boland, A., Kuzuoğlu-Öztürk, D., Bawankar, P., Loh, B., Chang, C.-T., Weichenrieder, O., Izaurralde, E., 2014. A DDX6-CNOT1 Complex and W-Binding Pockets in CNOT9 Reveal Direct Links between miRNA Target Recognition and Silencing. *Molecular Cell* 54, 737–750. <https://doi.org/10.1016/j.molcel.2014.03.034>
- Chu, C., Rana, T.M., 2006. Translation Repression in Human Cells by MicroRNA-Induced Gene Silencing Requires RCK/p54. *PLoS Biol* 4, e210. <https://doi.org/10.1371/journal.pbio.0040210>
- Cong, L., Ran, F.A., Cox, D., Lin, S., Barretto, R., Habib, N., Hsu, P.D., Wu, X., Jiang, W., Marraffini, L.A., Zhang, F., 2013. Multiplex Genome Engineering Using CRISPR/Cas Systems. *Science* 339, 819–823. <https://doi.org/10.1126/science.1231143>
- Corley, M., Burns, M.C., Yeo, G.W., 2020. How RNA-Binding Proteins Interact with RNA: Molecules and Mechanisms. *Molecular Cell* 78, 9–29. <https://doi.org/10.1016/j.molcel.2020.03.011>
- Coucovanis, E.C., Sherwood, S.W., Carswell-Crumpton, C., Spack, E.G., Jones, P.P., 1993. Evidence That the Mechanism of Prenatal Germ Cell Death in the Mouse Is Apoptosis. *Experimental Cell Research* 209, 238–247. <https://doi.org/10.1006/excr.1993.1307>
- Decker, C.J., Parker, R., 2012. P-Bodies and Stress Granules: Possible Roles in the Control of Translation and mRNA Degradation. *Cold Spring Harb Perspect Biol* 4, a012286. <https://doi.org/10.1101/cshperspect.a012286>
- Di Tommaso, P., Moretti, S., Xenarios, I., Orobittg, M., Montanyola, A., Chang, J.-M., Taly, J.-F., Notredame, C., 2011. T-Coffee: a web server for the multiple sequence alignment of protein and RNA sequences using structural information and homology extension. *Nucleic Acids Res* 39, W13–W17. <https://doi.org/10.1093/nar/gkr245>
- Dodson, A.E., Kennedy, S., 2020. Phase Separation in Germ Cells and Development. *Developmental Cell* S1534580720307061. <https://doi.org/10.1016/j.devcel.2020.09.004>
- Duszczuk, M.M., Wischniewski, H., Kazeeva, T., Loughlin, F.E., von Schroetter, C., Pradère, U., Hall, J., Ciaudo, C., Allain, F.H.-T., 2019. The solution structure of Dead End bound to AU-rich RNA reveals an unprecedented mode of tandem RRM-RNA recognition required for mRNA regulation (preprint). *Molecular Biology*. <https://doi.org/10.1101/572156>
- Dymecki, S.M., 1996. Flp recombinase promotes site-specific DNA recombination in embryonic stem cells and transgenic mice. *PNAS* 93, 6191–6196. <https://doi.org/10.1073/pnas.93.12.6191>
- Eulalio, A., Behm-Ansmant, I., Izaurralde, E., 2007. P bodies: at the crossroads of post-transcriptional pathways. *Nature Reviews Molecular Cell Biology* 8, 9–22. <https://doi.org/10.1038/nrm2080>
- Franks, T.M., Lykke-Andersen, J., 2008. The Control of mRNA Decapping and P-Body Formation. *Mol Cell* 32, 605–615. <https://doi.org/10.1016/j.molcel.2008.11.001>
- Gross-Thebing, T., Raz, E., 2020. Dead end and Detour: The function of the RNA-binding protein Dnd in posttranscriptional regulation in the germline, in: *Current Topics in Developmental Biology*. Elsevier, pp. 181–208. <https://doi.org/10.1016/bs.ctdb.2019.12.003>
- Haraguchi, S., Tsuda, M., Kitajima, S., Sasaoka, Y., Nomura-Kitabayashid, A., Kurokawa, K., Saga, Y., 2003. nanos1: a mouse nanos gene expressed in the central nervous system is dispensable for normal development. *Mechanisms of Development* 120, 721–731. [https://doi.org/10.1016/S0925-4773\(03\)00043-1](https://doi.org/10.1016/S0925-4773(03)00043-1)
- Ito, K., Takahashi, A., Morita, M., Suzuki, T., Yamamoto, T., 2011. The role of the CNOT1 subunit of the CCR4-NOT complex in mRNA deadenylation and cell viability 9.
- Kato, Y., Katsuki, T., Kokubo, H., Masuda, A., Saga, Y., 2016. Dazl is a target RNA suppressed by mammalian NANOS2 in sexually differentiating male germ cells. *Nat Commun* 7. <https://doi.org/10.1038/ncomms11272>
- Kedersha, N., Stoecklin, G., Ayodele, M., Yacono, P., Lykke-Andersen, J., Fritzler, M.J., Scheuner, D., Kaufman, R.J., Golan, D.E., Anderson, P., 2005. Stress granules and processing bodies are dynamically linked sites of mRNP remodeling. *J Cell Biol* 169, 871–884. <https://doi.org/10.1083/jcb.200502088>
- Kelley, L.A., Mezulis, S., Yates, C.M., Wass, M.N., Sternberg, M.J.E., 2015. The Phyre2 web portal for protein modeling, prediction and analysis. *Nat Protoc* 10, 845–858. <https://doi.org/10.1038/nprot.2015.053>

- Kumari, P., Bhavesh, N.S., 2020. Human DND1-RRM2 forms a non-canonical domain swapped dimer (preprint). *Biophysic*s. <https://doi.org/10.1101/2020.03.05.978023>
- Laible, M., Boonrod, K., 2009. Homemade site directed mutagenesis of whole plasmids. *J Vis Exp*. <https://doi.org/10.3791/1135>
- Licatalosi, D.D., 2016. Roles of RNA-binding Proteins and Post-transcriptional Regulation in Driving Male Germ Cell Development in the Mouse, in: Yeo, G.W. (Ed.), *RNA Processing: Disease and Genome-Wide Probing*, Advances in Experimental Medicine and Biology. Springer International Publishing, Cham, pp. 123–151. https://doi.org/10.1007/978-3-319-29073-7_6
- Lolicato, F., Marino, R., Paronetto, M.P., Pellegrini, M., Dolci, S., Geremia, R., Grimaldi, P., 2008. Potential role of Nanos3 in maintaining the undifferentiated spermatogonia population. *Developmental Biology* 313, 725–738. <https://doi.org/10.1016/j.ydbio.2007.11.011>
- Nguyen, D.H., Soygur, B., Peng, S.-P., Malki, S., Hu, G., Laird, D.J., 2020. Apoptosis in the fetal testis eliminates developmentally defective germ cell clones. *Nature Cell Biology* 1–13. <https://doi.org/10.1038/s41556-020-00603-8>
- Nishi, H., Hashimoto, K., Panchenko, A.R., 2011. Phosphorylation in Protein-Protein Binding: Effect on Stability and Function. *Structure* 19, 1807–1815. <https://doi.org/10.1016/j.str.2011.09.021>
- Notredame, C., Higgins, D.G., Heringa, J., 2000. T-coffee: a novel method for fast and accurate multiple sequence alignment. Edited by J. Thornton. *Journal of Molecular Biology* 302, 205–217. <https://doi.org/10.1006/jmbi.2000.4042>
- O, O., K, S., C, A., Dg, H., C, N., 2004. 3DCoffee: combining protein sequences and structures within multiple sequence alignments. *J Mol Biol* 340, 385–395. <https://doi.org/10.1016/j.jmb.2004.04.058>
- Poirot, O., Suhre, K., Abergel, C., O'Toole, E., Notredame, C., 2004. 3DCoffee@igs: a web server for combining sequences and structures into a multiple sequence alignment. *Nucleic Acids Res* 32, W37–W40. <https://doi.org/10.1093/nar/gkh382>
- Rucker, E.B., Dierisseau, P., Wagner, K.U., Garrett, L., Wynshaw-Boris, A., Flaws, J.A., Hennighausen, L., 2000. Bcl-x and Bax regulate mouse primordial germ cell survival and apoptosis during embryogenesis. *Molecular endocrinology (Baltimore, Md.)* 14, 1038–1052. <https://doi.org/10.1210/me.14.7.1038>
- Saba, R., Kato, Y., Saga, Y., 2014. NANOS2 promotes male germ cell development independent of meiosis suppression. *Developmental Biology* 385, 32–40. <https://doi.org/10.1016/j.ydbio.2013.10.018>
- Sada, A., Suzuki, A., Suzuki, H., Saga, Y., 2009. The RNA-Binding Protein NANOS2 Is Required to Maintain Murine Spermatogonial Stem Cells. *Science* 325, 1394–1398. <https://doi.org/10.1126/science.1172645>
- Saga, Y., 2008. Sexual development of mouse germ cells: Nanos2 promotes the male germ cell fate by suppressing the female pathway: Sexual development of mouse germ cells. *Development, Growth & Differentiation* 50, S141–S147. <https://doi.org/10.1111/j.1440-169X.2008.01009.x>
- Schindelin, J., Arganda-Carreras, I., Frise, E., Kaynig, V., Longair, M., Pietzsch, T., Preibisch, S., Rueden, C., Saalfeld, S., Schmid, B., Tinevez, J.-Y., White, D.J., Hartenstein, V., Eliceiri, K., Tomancak, P., Cardona, A., 2012. Fiji: an open-source platform for biological-image analysis. *Nature Methods* 9, 676–682. <https://doi.org/10.1038/nmeth.2019>
- Sheth, U., 2003. Decapping and Decay of Messenger RNA Occur in Cytoplasmic Processing Bodies. *Science* 300, 805–808. <https://doi.org/10.1126/science.1082320>
- Shimada, R., Kiso, M., Saga, Y., 2019. ES-mediated chimera analysis revealed requirement of DDX6 for NANOS2 localization and function in mouse germ cells. *Sci Rep* 9, 515. <https://doi.org/10.1038/s41598-018-36502-0>
- Shimada, R., Koike, H., Hirano, T., Saga, Y., 2020. NANOS2 suppresses the cell cycle by repressing mTORC1 activators in embryonic male germ cells. *bioRxiv* 55. <https://doi.org/10.1101/2020.09.23.310912>
- Shirai, Y.-T., Suzuki, T., Morita, M., Takahashi, A., Yamamoto, T., 2014. Multifunctional roles of the mammalian CCR4–NOT complex in physiological phenomena. *Front. Genet.* 5. <https://doi.org/10.3389/fgene.2014.00286>
- Stoecklin, G., Kedersha, N., 2013. Relationship of GW/P-Bodies with Stress Granules, in: Chan, E.K.L., Fritzler, M.J. (Eds.), *Ten Years of Progress in GW/P Body Research*, Advances in Experimental Medicine

- and Biology. Springer, New York, NY, pp. 197–211. https://doi.org/10.1007/978-1-4614-5107-5_12
- Suzuki, A., Niimi, Y., Saga, Y., 2014. Interaction of NANOS2 and NANOS3 with different components of the CNOT complex may contribute to the functional differences in mouse male germ cells. *Biology Open* 3, 1207–1216. <https://doi.org/10.1242/bio.20149308>
- Suzuki, A., Niimi, Y., Shinmyozu, K., Zhou, Z., Kiso, M., Saga, Y., 2016. Dead end1 is an essential partner of NANOS2 for selective binding of target RNAs in male germ cell development. *EMBO reports* 17, 37–46. <https://doi.org/10.15252/embr.201540828>
- Suzuki, A., Saba, R., Miyoshi, K., Morita, Y., Saga, Y., 2012. Interaction between NANOS2 and the CCR4-NOT Deadenylation Complex Is Essential for Male Germ Cell Development in Mouse. *PLOS ONE* 7, e33558. <https://doi.org/10.1371/journal.pone.0033558>
- Suzuki, A., Saga, Y., 2008. Nanos2 suppresses meiosis and promotes male germ cell differentiation. *Genes Dev.* 22, 430–435. <https://doi.org/10.1101/gad.1612708>
- Suzuki, A., Tsuda, M., Saga, Y., 2007. Functional redundancy among Nanos proteins and a distinct role of Nanos2 during male germ cell development. *Development* 134, 77–83. <https://doi.org/10.1242/dev.02697>
- Suzuki, H., Saba, R., Sada, A., Saga, Y., 2010. The Nanos3-3'UTR Is Required for Germ Cell Specific NANOS3 Expression in Mouse Embryos. *PLoS ONE* 5, e9300. <https://doi.org/10.1371/journal.pone.0009300>
- Suzuki, H., Tsuda, M., Kiso, M., Saga, Y., 2008. Nanos3 maintains the germ cell lineage in the mouse by suppressing both Bax-dependent and -independent apoptotic pathways. *Dev. Biol.* 318, 133–142. <https://doi.org/10.1016/j.ydbio.2008.03.020>
- Tsuda, M., 2003. Conserved Role of nanos Proteins in Germ Cell Development. *Science* 301, 1239–1241. <https://doi.org/10.1126/science.1085222>
- Wright, D., Kiso, M., Saga, Y., 2020. Genetic and structural analysis of the *in vivo* functional redundancy between murine NANOS2 and NANOS3. *Development* dev.191916. <https://doi.org/10.1242/dev.191916>
- Yamane, M., Ohtsuka, S., Matsuura, K., Nakamura, A., Niwa, H., 2018. Overlapping functions of Krüppel-like factor family members: targeting multiple transcription factors to maintain the naïve pluripotency of mouse embryonic stem cells. *Development* 145, dev162404. <https://doi.org/10.1242/dev.162404>
- Zhou, Z., Shirakawa, T., Ohbo, K., Sada, A., Wu, Q., Hasegawa, K., Saba, R., Saga, Y., 2015. RNA Binding Protein Nanos2 Organizes Post-transcriptional Buffering System to Retain Primitive State of Mouse Spermatogonial Stem Cells. *Developmental Cell* 34, 96–107. <https://doi.org/10.1016/j.devcel.2015.05.014>

Figure Legends

Figure 1. Establishment of mutant mice

A) Schema of the creation of *Nanos2^{mcherry}* mice. The neomycin cassette was removed by crossing with *Rosa-Flp* mice¹⁵. To create *Nanos2^{mcherry}*, the mice were crossed with CAG-Cre mice to remove *3xFlag-Nanos2*. B) Schema of the creation of *Nanos3* cKO mice. Tamoxifen was injected to remove *3xF-Nanos3*. C) Testis sections from E13.5 *Nanos3* cKO mice administered tamoxifen at E11.5 were stained with anti-FLAG (green) and anti-E-cadherin (red) to assess the Cre recombination efficiency. No germ cells in Cre+ mice expressed 3xF-NANOS3 at E13.5. DNA was labeled with DAPI (blue).

Figure 2. The conditional knockout of *Nanos3* does not affect male differentiation.

A) Sections of E13.5-E15.5 control and *Nanos3* cKO testes were stained with antibody against E-cadherin (ECAD) to mark germ cells. Scale bar 50 μ m. A 2x enlarged image of the selected area is shown in each figure. B) Quantification of germ cell numbers in E13.5-E15.5 control and *Nanos3* cKO testes (for all n=3). C) Sections of E14.5 control and *Nanos3* cKO testes were stained with antibodies against E-cadherin and DNMT3L to mark male-type differentiation. Scale bar 30 μ m. DNA was stained with DAPI (blue). D) E15.5 control, *Nanos3* cKO, and *Nanos2* KO testis sections were stained with an antibody against DAZL, a reported target of NANOS2. Scale bar 30 μ m. E) Quantification of DAZL immunostaining for E15.5 control, *Nanos3* cKO, and *Nanos2* KO testes. **** indicates significant difference with $P < 0.0001$ by the unpaired Student's t-test.

Figure 3. Conditional double knockout of *Nanos2/3* leads to rapid germ cell death during the sexual differentiation stage.

A) Sections of E13.5-E16.5 control and *Nanos2/3* dKO testes were stained with antibodies against E-cadherin (red) and SOX9 (white) to mark germ cells and Sertoli cells, respectively. DNA was stained with DAPI (blue). Note the rapid loss of germ cells in the dKO between E13.5 and E14.5. Scale bar 50 μ m. B) Germ cell/ Sertoli cell ratio in control and dKO testes (control and dKO E14.5-E16.5 n=3, dKO E13.5 n=3). **** indicates significant difference with $P < 0.0001$ by the unpaired Student's t-test. C) E14.5 wild-type, *Nanos2* KO and dKO testis sections were stained with antibodies against cleaved PARP (white) and E-cadherin (red). Scale bar 30 μ m. D) Quantification of C-PARP signals in E14.5 wild-type, *Nanos2* KO and dKO testis sections. *** indicates significant difference with $P < 0.0004$ by the unpaired Student's t-test. E) Sections of E14.5 control, *Nanos2* KO, and *Nanos2/3* dKO testes were stained with antibodies against STRA8 (green) and E-cadherin (magenta). DNA was stained with DAPI (blue). Scale bar 50 μ m. F) Sections of E14.5 control, *Nanos2* KO, and *Nanos2/3* dKO testes were stained with antibodies against Ki-67 (white) and E-cadherin (red). Scale bar 10 μ m.

Figure 4. Loss of NANOS causes the loss of DND1 protein

A) Sections of testes from E13.5 and E14.5 *Nanos2/3* dKO embryos were stained with antibodies against DND1 (white) and E-cadherin (red). Scale bar 50 μ m. Enlarged images of selections in the white squares are shown on the right. Scale bar 10 μ m. B) DND1 expression in wild-type, *Nanos2* KO and *Nanos3* cKO germ cells. Sections of testes from

E14.5 wild-type, *Nanos2* KO or *Nanos3* cKO embryos were stained with anti-DND1 (red). DNA was stained with DAPI (blue). Scale bar 20 μ m. C) Single-cell RNA sequencing results for *Actb* and *Dnd1* using E13.5 and E14.5 control and *Nanos2* KO germ cells (data were obtained from Shimada et al. 2020 preprint). Violin plots were generated using the Seurat package for R (Butler et al., 2018). Black dots indicate the median

Figure 5. Assessment of DND1 expression in cultured cells and mouse ESCs

A) Western blotting of HEK293T cells expressing HA-DND1 alone or together with 3xF-NANOS2 cultured with or without cycloheximide for the indicated times. β -tubulin was used as a control. B) Western blotting of HEK293T cells expressing HA-DND1 alone or together with 3xF-NANOS2, NANOS3 or NANOS2-3C cultured with or without cycloheximide for the indicated times. β -tubulin was used as a control. C) Western blotting of inducible mouse ESCs cultured with or without cycloheximide for the indicated times. β -tubulin was used as a control.

Figure 6. Chimeric proteins failed to initiate the male pathway.

A) Comparison of NANOS2 and NANOS3 proteins by protein structural information using the T-coffee algorithm Expresso (Armougom et al., 2006; Di Tommaso et al., 2011; Notredame et al., 2000; O et al., 2004; Poirot et al., 2004). Red indicates a high degree of structural similarity, yellow is moderate and green is low similarity. The key domains are outlined; The N-terminal in green, zinc finger in blue and C-terminal in yellow. Note that the NANOS3 C-terminal is 46 amino acids longer than the NANOS2 C-terminal. B) Diagram of wild-type NANOS2 and NANOS3 protein domains (NANOS2 in orange,

NANOS3 in purple) and diagram of chimeric proteins made by interchanging NANOS2 and NANOS3 domains (top: 3xF-Nanos2N58-Nanos3-ZF(Δ C46), bottom: 3xF-Nanos3N54-Nanos2-ZF). For 3xF-Nanos2N58-Nanos3-ZF(Δ C46), the last 46 amino acids of the NANOS3 C-terminal were removed. C) A) Comparison of protein expression among 3xF NANOS2, 3xF-NANOS2N58-NANOS3-ZF(Δ C46) and 3xF-NANOS3N54-NANOS2-ZF. E15.5 testis sections were stained with anti-FLAG and anti-E-cadherin. Scale bar 40 μ m. D) Sections of E15.5 chimeric testes derived from ES cells containing 3xF-Nanos2N58-Nanos3-ZF(Δ C46) (top) or 3xF-Nanos3N54-Nanos2-ZF (bottom) were stained with antibodies against FLAG (green) and DNMT3L (magenta). DNA was labeled with DAPI (blue). Scale bar 40 μ m. E) Quantification of DNMT3L immunostaining in 3xF-Nanos2N58-Nanos3-ZF(Δ C46) and 3xF-Nanos3N54-Nanos2-ZF chimeric testes. F) Sections from E15.5 and E17.5 3xF-Nanos2N58-Nanos3-ZF(Δ C46) (top) or 3xF-Nanos3N54-Nanos2-ZF (bottom) testes were stained with antibodies against FLAG (green), STRA8 (red), and a germ cell marker (magenta). DNA was labeled with DAPI (blue). Scale bar 50 μ m. Compared with wild-type cells, FLAG-positive cells highly express STRA8 at E17.5. **** indicates significant difference with $P < 0.0001$ by the unpaired Student's t-test

Figure 7. *Nanos2* KO phenotypes are observed in chimeric germ cells.

A) Endogenous NANOS3 is still upregulated in chimeric germ cells. Sections of testes from E15.5 3xF-Nanos2N58-Nanos3-ZF(Δ C46) (top) or 3xF-Nanos3N54-Nanos2-ZF (bottom) were stained with antibodies against FLAG (green) and NANOS3 (red). DNA was

labeled with DAPI (blue). Scale bar 10 μ m. B) Western blotting of HEK293T cells transfected with the indicated proteins using anti-NANOS3 antibody. This antibody detects the C-terminal of NANOS3, and therefore can be used to assess endogenous NANOS3 expression in chimera. C) Sections of E15.5 chimeric testes derived from ES cells containing 3xF-Nanos2N58-Nanos3-ZF(Δ C46) (top) or 3xF-Nanos3N54-Nanos2-ZF (bottom) were stained with antibodies against FLAG (green) and DAZL (magenta). White arrows in enlarged areas selected in white boxes indicate wild-type cells and yellow arrowheads indicate mutant germ cells. DNA was labeled with DAPI (blue). Scale bar 40 μ m. D) Quantification of DAZL immunostaining in 3xF-Nanos2N58-Nanos3-ZF(Δ C46) and 3xF-Nanos3N54-Nanos2-ZF chimeric testes. **** indicates significant difference with $P < 0.0001$ by the unpaired Student's t-test

Figure 8. P-body localization of DND1 and chimeric proteins

A) Sections of testes from E15.5 3xF-Nanos2N58-Nanos3-ZF(Δ C46) (top) or 3xF-Nanos3N54-Nanos2-ZF (bottom) were stained with antibodies for FLAG (green), indicating mutant germ cells, and DND1 (magenta), which is expressed in both mutant and wild-type germ cells. White arrowheads indicate merged DND1 and FLAG foci in chimeric germ cells. Asterisks indicate examples of wild-type cells. DNA was labeled with DAPI (blue). Scale bar 10 μ m. B) Sections of testes from E15.5 3xF-Nanos2N58-Nanos3-ZF(Δ C46) (top) or 3xF-Nanos3N54-Nanos2-ZF (bottom) chimeras were stained with antibodies against FLAG (green), DDX6 (white) and DND1 (red). FLAG-positive germ cells express the indicated mutant protein, whereas FLAG-negative cells are wild-type,

expressing wild-type NANOS2. In chimeric mice, these cells coexist in the same testis. DNA was labeled with DAPI (blue). Scale bar 5 μ m. C) The intensity of DND1 immunofluorescence images shown in B was intentionally increased to visualize granules. FLAG and DDX6 signals are unchanged from those in B. P-bodies merged with FLAG and DND1 are indicated by arrowheads.

Figure 9. DND1 strongly binds the NANOS2 ZF, but not the NANOS3 ZF.

A) Quantification of DND1 immunostaining in 3xF-Nanos2N58-Nanos3-ZF(Δ C46) and 3xF-Nanos3N54-Nanos2-ZF chimeric testes. **** indicates significant difference with $P < 0.0001$ by the unpaired Student's t-test. B) Cultured HEK293T cells were transfected with HA-DND1 and FLAG-tagged NANOS2, NANOS3, or mutant proteins. Forty-eight hours after transfection, cells were collected and used for immunoprecipitation with anti-FLAG beads. Co-precipitates were analyzed by Western blotting with anti-FLAG and anti-HA antibodies. Asterisk indicates 3xF-NANOS2N58-NANOS3-ZF(Δ C46), which was hardly expressed in HEK293T cells.

Figure 10. Mouse NANOS3 cannot strongly bind DND1

A) CCHC-CCHC zinc finger domains of NANOS2 and NANOS3 are aligned and compared by protein structural information. Blue arrows indicate amino acids changed to make point mutants. B, C) Cultured HEK293T cells were transfected with HA-DND1 and FLAG-tagged NANOS2, NANOS3, or NANOS2 or NANOS3 point mutants. Forty-eight hours after transfection, cells were collected and used for immunoprecipitation with anti-FLAG beads. Co-precipitates were analyzed by Western blotting with anti-FLAG and anti-

HA antibodies. Representative blots of triplicate experiments are shown. D) Comparison of mouse NANOS2, NANOS2 Y111F and NANOS3 zinc finger domains. Three-dimensional models were created using amino acid sequences of the respective proteins in the Phyre2 engine. Orange indicates cysteine and blue indicates histidine comprising the CCHC motif. The red amino acid is the position equivalent to Y111 in NANOS2, i.e., F107 in mouse NANOS3. When NANOS2 Y111 is mutated to F111, the side chain orientation becomes similar to that of NANOS3 F107.

Figure 11. Mouse NANOS3 cannot strongly bind CNOT1

A) Comparison of NANOS3 NIM sequences for several species. Asterisks indicate amino acids reported to be required for CNOT1 interaction (FWY). The red box indicates the NIMs for mouse NANOS2 and NANOS3, and human NANOS3. B) Each purified MBP-fusion protein was mixed with CNOT1-3-expressing *E.coli* lysate and then added to Gluthione Sepharose beads. The beads were boiled with SDS-PAGE loading buffer and run on acrylamide gels for CBB staining for CNOT1-3 or Western blotting with anti-MBP. C) mNANOS-NIM, mNANOS-NIM N-D, and huNANOS3-NIM pulldown. Asterisk indicates background expressed MBP tag, which was not pulled down.

Figure 12. NANOS3 and DND1 do not colocalize in NIH3T3 cells

A) Immunostaining of NIH3T3 cells expressing 3xF-NANOS3 (green) and HA-DND1 (magenta). P-bodies were stained with an antibody against DDX6 (white). DNA was stained with DAPI (blue). Enlarged images of the boxed area are shown on the right. Magnification 100x. Scale bars 5 μm , 1 μm . B) E15.5 WT and *Nanos2* KO testes were

stained with antibodies against NANOS3 (magenta) and DND1 (green). DNA was stained with DAPI (blue). Magnification 200x. Scale bar 2 μ m.

Figure 13. Establishment of the dCas13 system for imaging mRNA

A. Schema for imaging of stress granules and mRNA using dLwaCas13a. The Cas13 construct is taken from Abudayyeh et al. B. Images of transfected cells after adding arsenite. Left shows cells with a non-targeting guide, middle shows cells with no guide, and right is a cell with the ACTB guide. Note that without a guide, this dCas13 construct is not translocated to the cytoplasm. The localization pattern is similar to that reported in the original paper. C. Images of NIH3T3 cells transfected with or without *Dazl* and guide 1, which resulted in signal even without *Dazl*. A cartoon of the location of the guide target sequence is shown on the right. D. Images of NIH3T3 cells transfected with or without *Dazl* and guide 2, which was specific for *Dazl*. The location of the *Dazl* guide target sequence is shown on the right.

Figure 14. NANOS2 and DND1 alter the localization pattern of *Dazl* mRNA

A. Western blotting of ciN2D13T3 cells with and without doxycycline confirming the induction of NANOS2 and DND1. B. Regulation of *Dazl* by NANOS2 is through the 3'UTR. Just the *Dazl* coding sequence did not lead to repression of protein expression upon the induction of NANOS2 and DND1. C. Schema of dCas13 system for visualizing *Dazl* mRNA live. D. A P-body containing *dazl* without doxycycline. Scale bar 1 μ m. E. NANOS2 and DND1 begin to be expressed from 5 hours after adding doxycycline. Magnification 200x. Scale bar 5 μ m. Insets of boxed areas show a 2x magnified image. F.

ViewRNA staining of *Dazl*. Without transfecting *Dazl*, there are no *Dazl* transcripts marked by dCas13 or ViewRNA probe. Without doxycycline, most *Dazl* is in the cytoplasm. After adding doxycycline, *Dazl* is localized inside of P-bodies. dCas13 (green) and ViewRNA probe (white) signal are both colocalized with P-bodies, as indicated by purple arrowheads. dCas13 was stained by anti-GFP, P-bodies were stained by an antibody against DDX6. DNA was stained by DAPI. Magnification 200x. Scale bar 5 μm . Enlarged images of boxed area show a 2x magnified image. G. Cytofluorograms for *dazl* vs DDX6 with or without doxycycline. The colored bars indicate which channels were assessed. The r value is the Coloc correlation coefficient.

Figure 15. NANOS2, DND1 and mRNA are all required for the formation of P-bodies

A. Super resolution microscopy image of P-bodies inside NIH3T3 transfected with NANOS2, HA-tagged DND1, and the dCas13 system. Immunostaining was performed using anti-NANOS2, anti-HA and anti-GFP. Scale bar 1 μm . B. Schema for 4-color live imaging using NIH3T3 cells. C. Images from 4-color live imaging. Yellow arrowheads indicate P-bodies containing all 4 components. White arrows indicate DND1 colocalized with *Dazl* alone. Note that NANOS2 does not colocalize with *Dazl* without DND1. Scale bar 2 μm . D. Live imaging screenshots. Yellow arrowheads indicate DND1 interacting with *Dazl* and NANOS2. The white arrow from time point 12 min 45 sec indicates DND1 newly binding *Dazl* without NANOS2. Scale bar 1 μm .

Figure 16. DND1 interacts with mRNA alone, whereas NANOS2 does not.

A. Representative cell expressing BFP2-NANOS2, dCas13 system and DCP1a-mi670. NANOS2 and *Dazl* only slightly colocalize to small DCP1a foci, shown by yellow arrowhead. The white arrow shows DCP1a only colocalized with *Dazl*. Blue is NANOS2, green is *Dazl* and white is DCP1a. Scale bar 2 μ m. B. Representative cell expressing DND1-tagRFP, dCas13 system and DCP1a-mi670. DND1 and *Dazl* are more highly colocalized throughout the cytoplasm, but there are few larger DCP1a foci indicated by yellow arrowheads. Red is DND1, green is *Dazl* and white is DCP1a. Scale bar 2 μ m.

Figure 17. Strong mRNA binding by DND1 is required for stable P-bodies

A. Representative cells expressing BFP2-NANOS2, DND1-tagRFP, dCas13 system and DCP1a-mi670. With both NANOS2 and DND1, large stable P-bodies are formed, with continuous *Dazl* recruitment. The arrowheads indicate P-bodies over time. Scale bar 5 μ m. The enlarged images of the boxed area over time are magnified 2x. B. Cytofluorograms for NANOS2 vs *Dazl* (left), *Dazl* vs DND1 (middle) and DND1 vs NANOS2 (right). The r value is the Coloc correlation coefficient. C. Representative cell expressing BFP2-NANOS2, DND1R98A-tagRFP, dCas13 system and DCP1a-mi670. There is little *Dazl* accumulation and P-bodies are unstable, differing from the wild-type case shown above. Arrowheads indicate small foci, which dissipate over time. Scale bar 5 μ m. The enlarged images of the boxed area over time are magnified 2x. D. Cytofluorograms for NANOS2 vs *Dazl* (left), *Dazl* vs DND1R98A (middle) and DND1R98A vs NANOS2 (right). The colored bars indicate which channels were assessed. The r value is the Coloc correlation coefficient. E. Representative cell expressing BFP2-NANOS2-ZM, DND1-tagRFP, and

dCas13 system. NANOS2-ZM cannot bind DND1 but forms artificial aggregates. Scale bar 5 μm . The enlarged images of the boxed area over time are magnified 2x. F.

Cytofluorograms for NANOS2-ZM vs *Dazl* (left), *Dazl* vs DND1 (middle) and DND1 vs NANOS2-ZM (right). The r value is the Coloc correlation coefficient.

Figure 18. CNOT1 recruitment by NANOS2 regulates target mRNA binding by DND1 and P-body formation

A. Comparison of CNOT1 recruitment in NIH3T3 cells expressing NANOS2 (top, blue) or del-N-NANOS2 (bottom, blue). *Dazl* is shown in green, DND1 is shown in red and CNOT1 is shown in white. In the wild-type case, all components colocalize with CNOT1, shown by yellow arrowheads. In the cell expressing del-N-NANOS2, del-N-NANOS2 is alone in the cytoplasm (yellow arrowheads) without DND1 or CNOT1 (white arrows). B. Comparison of DCP1a localization in NIH3T3 cells expressing NANOS2 (top, blue) or del-N-NANOS2 (bottom, blue). NANOS2 and DND1 are colocalized inside DCP1a foci (yellow arrowheads), whereas in the del-N-NANOS2 case, DND1 is located outside of DCP1a (yellow arrowheads) and has limited colocalization with del-N-NANOS2 (white arrows). C. Same as in A except comparing the DDX6 localization pattern. DDX6, NANOS2, *Dazl* and DND1 all colocalize (yellow arrowheads), but in the presence of del-N-NANOS2, DND1 colocalizes with DDX6 without *Dazl* (yellow arrowheads). Del-N-NANOS2 is mostly alone throughout the cytoplasm (white arrows). Scale bar 2 μm .

Figure 1

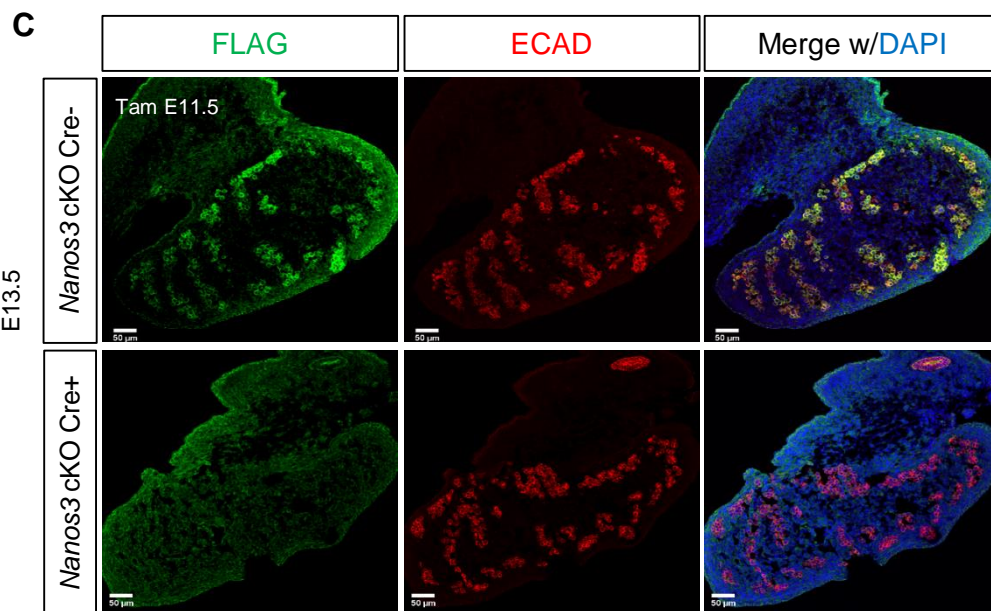
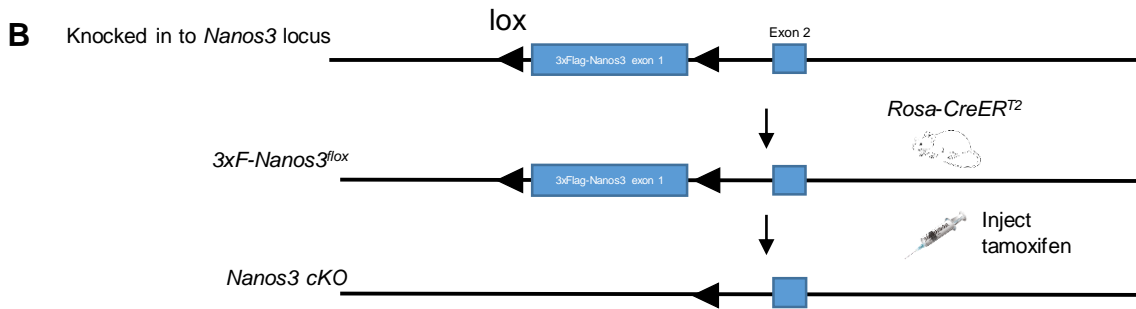
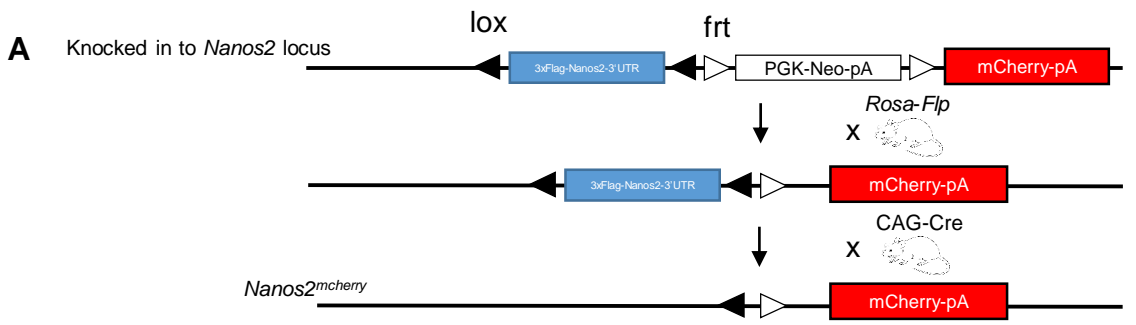


Figure 2

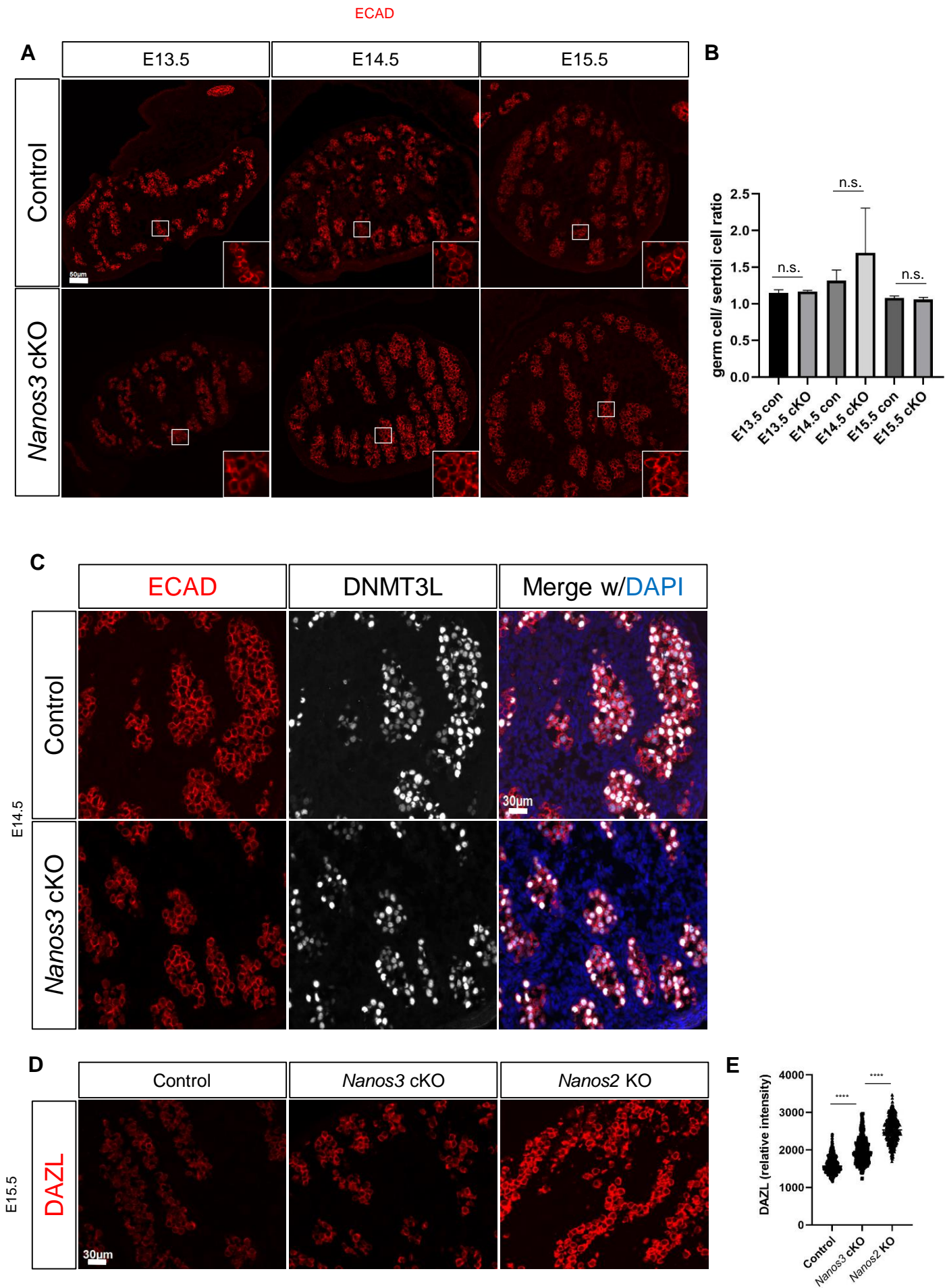


Figure 3

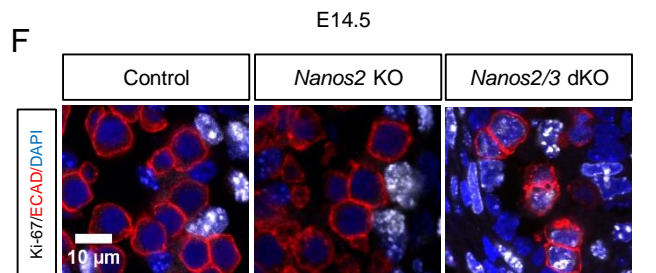
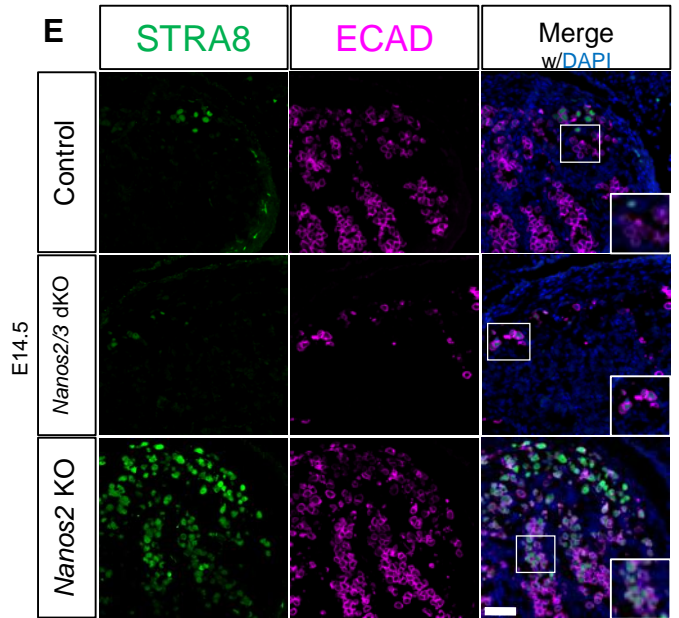
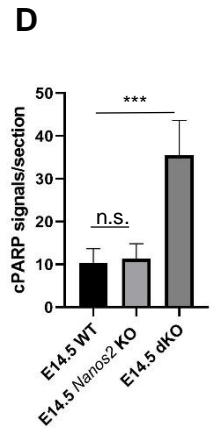
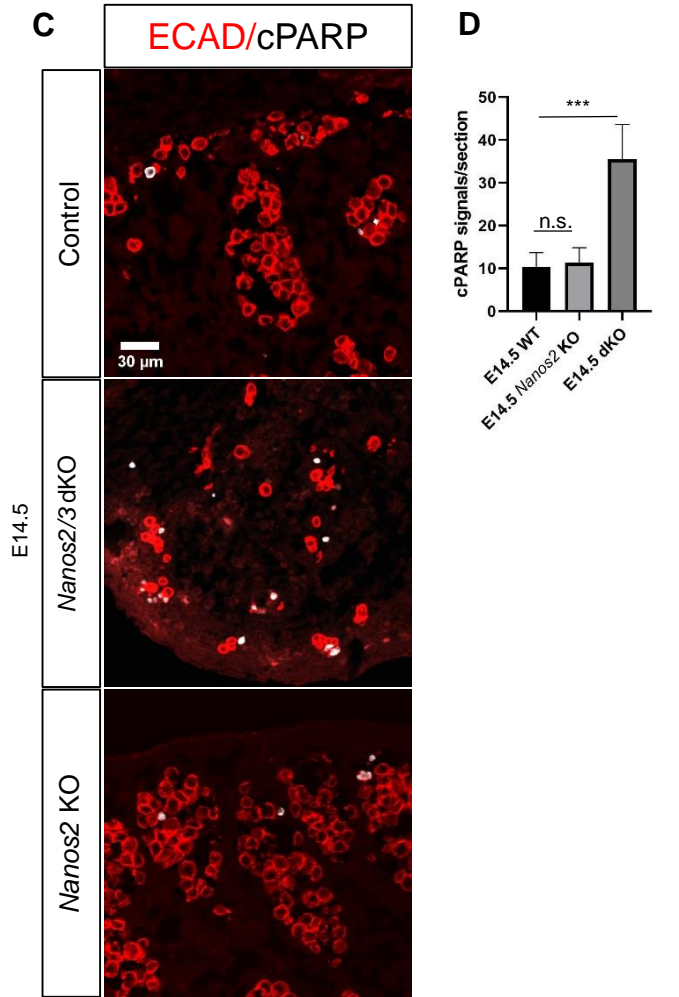
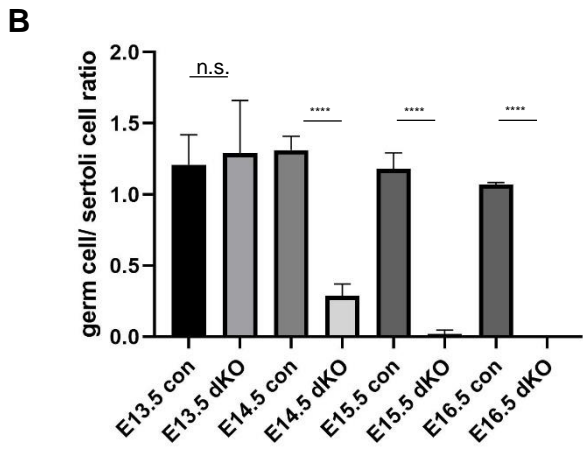
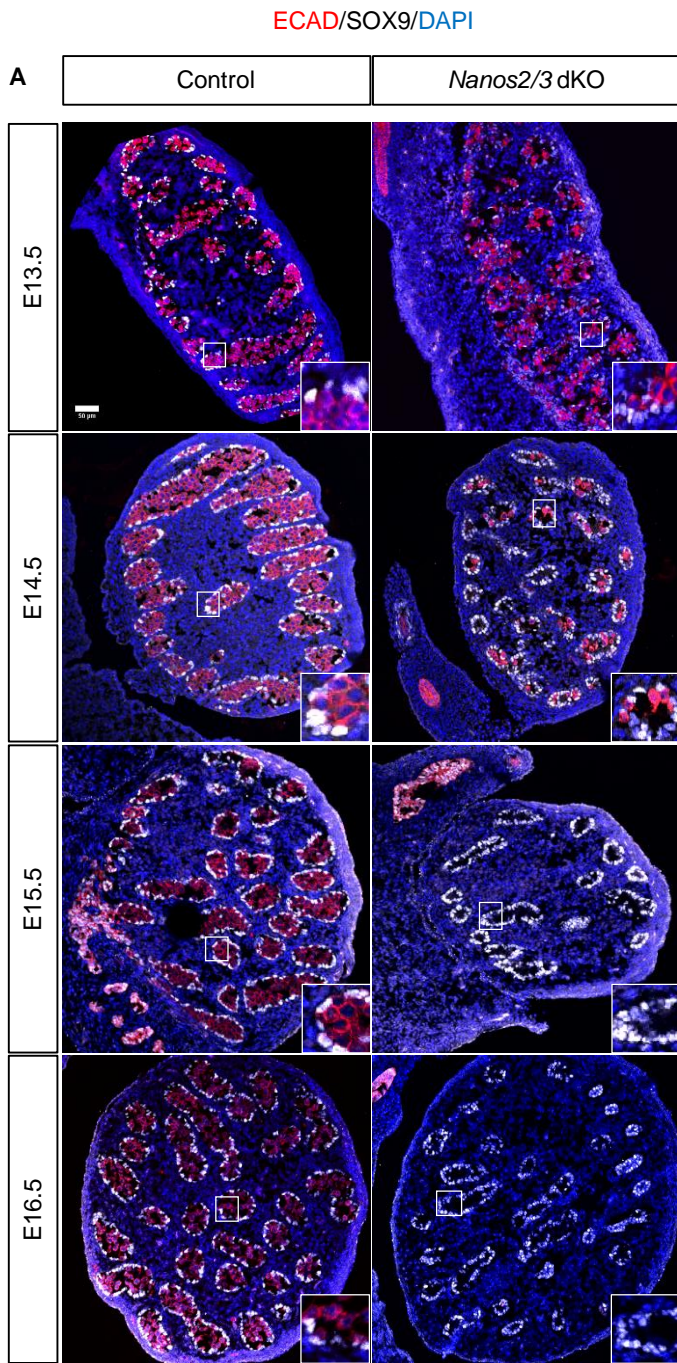


Figure 4

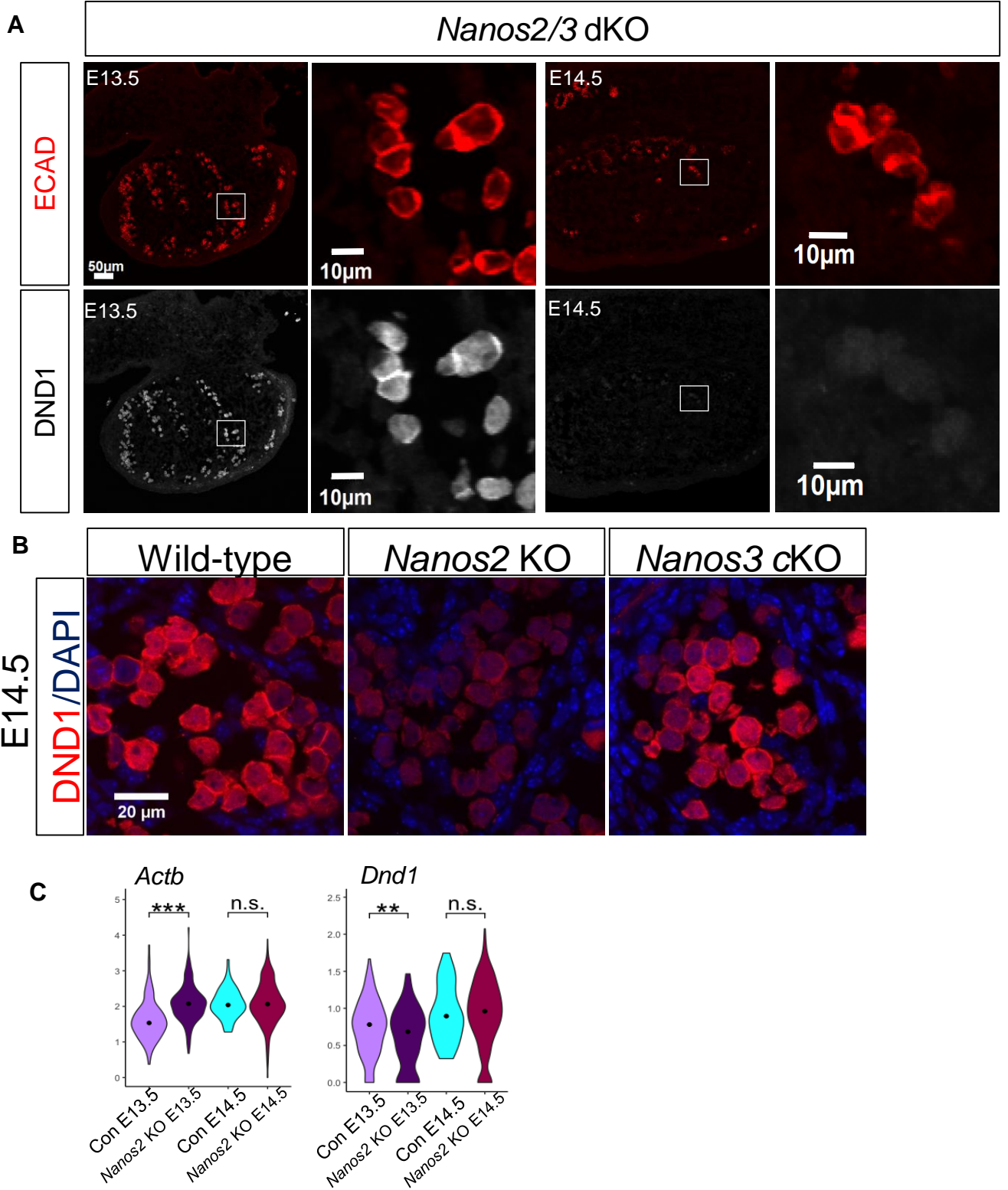
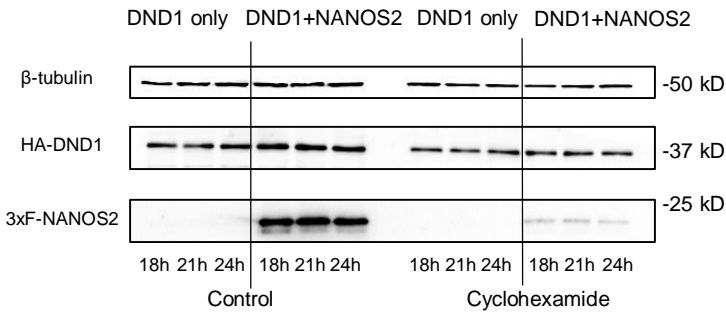
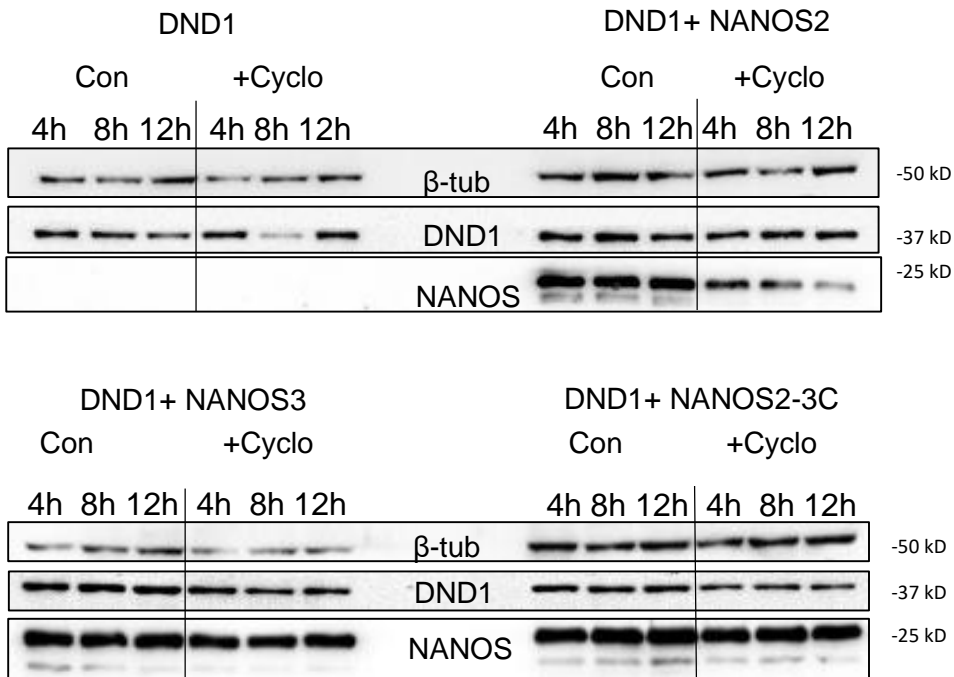


Figure 5

A



B



C

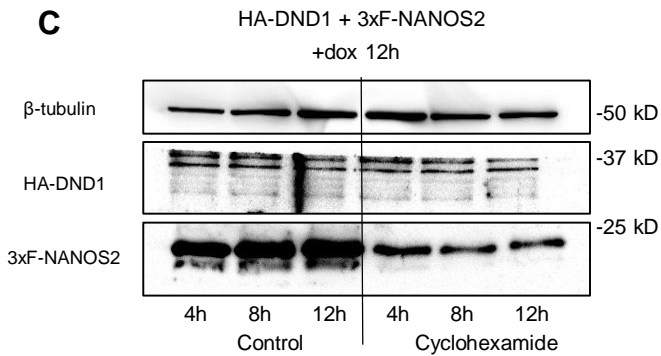
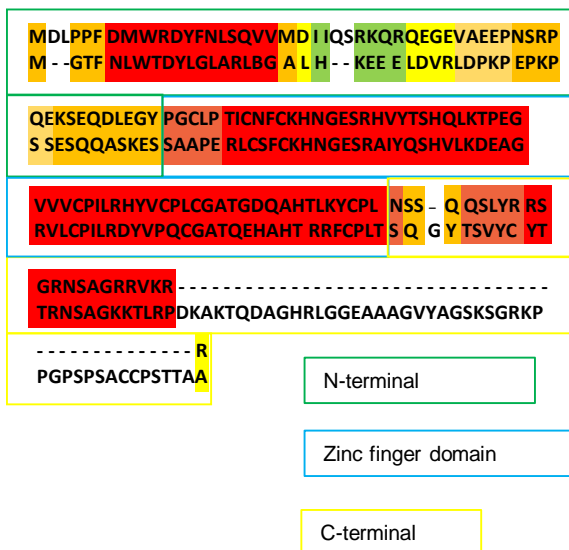


Figure 6

A

NANOS2
NANOS3



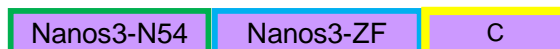
B

Wild-type proteins

NANOS2



NANOS3



Chimeric proteins

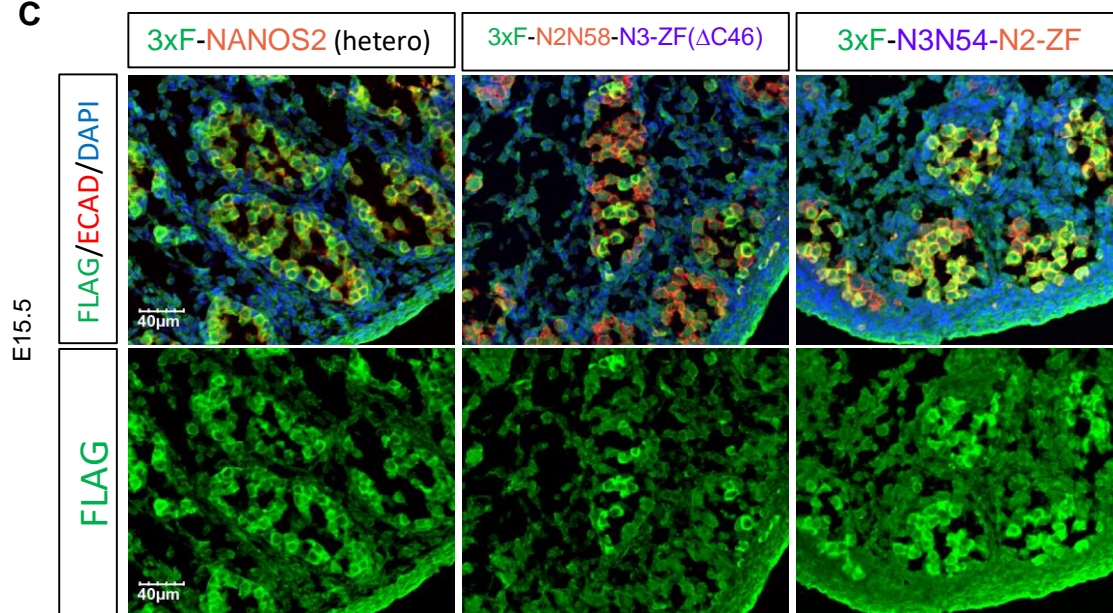
3xF-N2N58-N3-ZF(Δ C46)



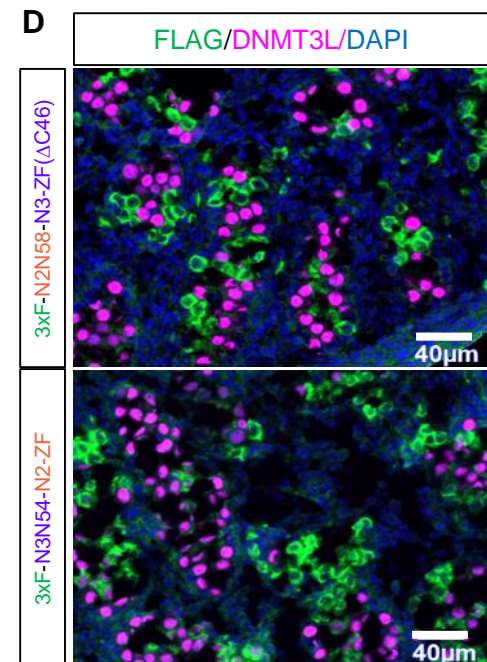
3xF-N3N54-N2-ZF



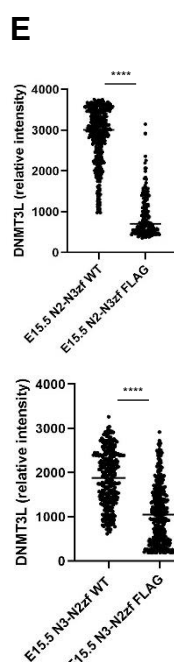
C



D



E



F

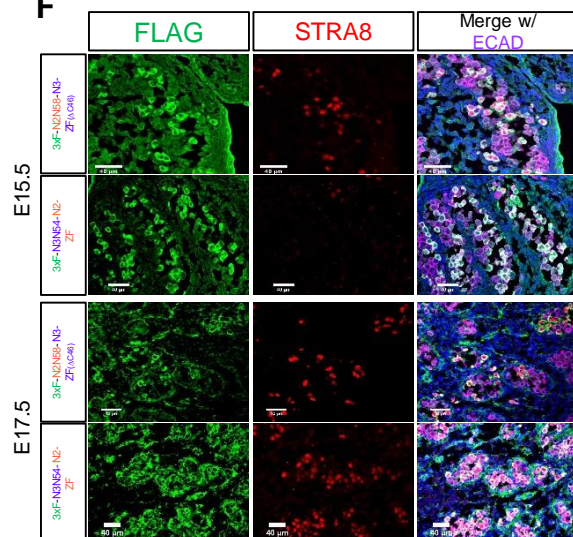


Figure 7

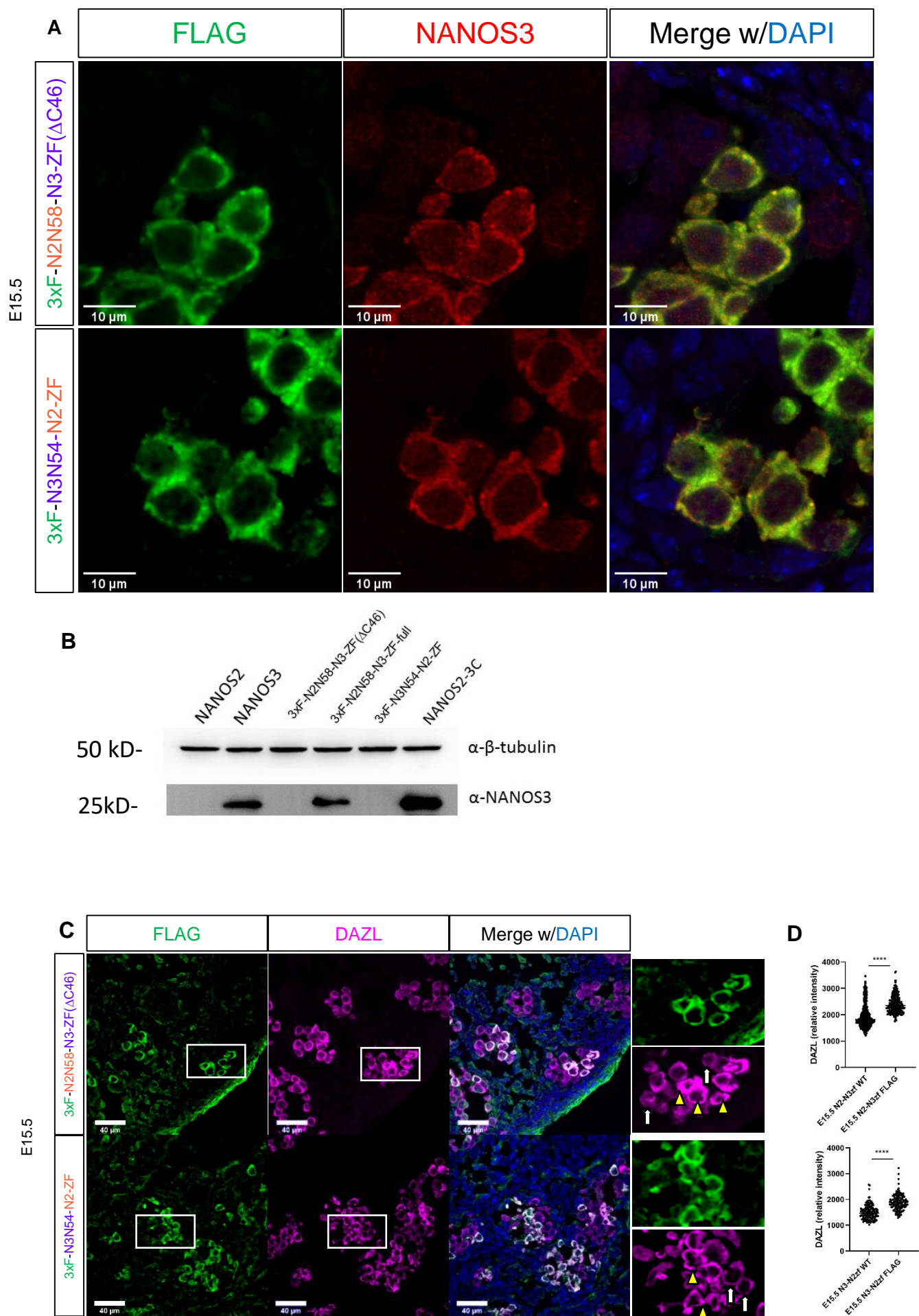


Figure 8

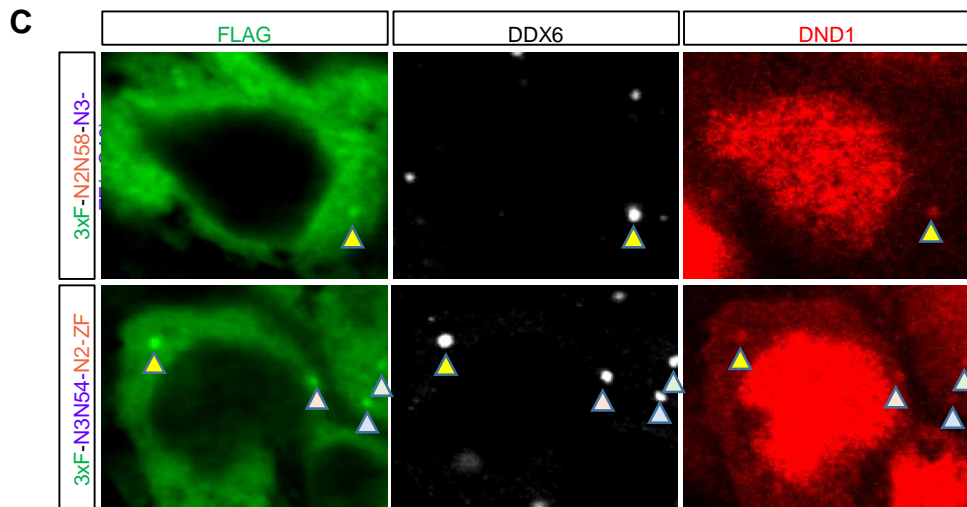
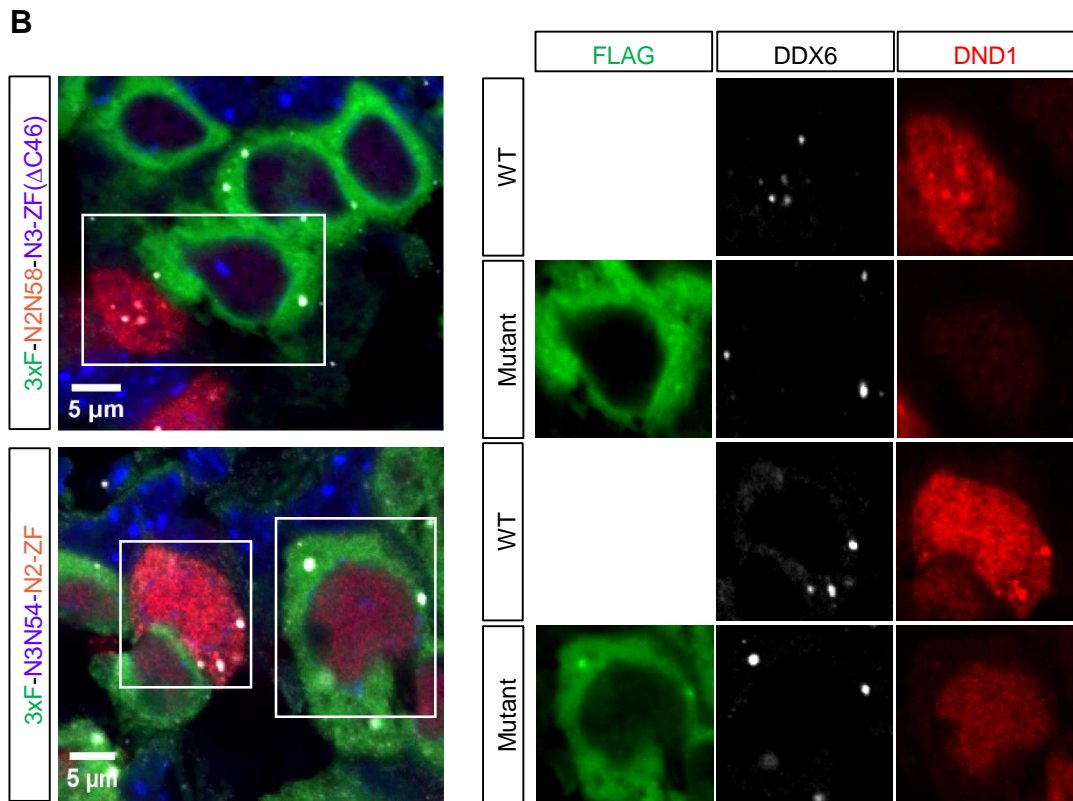
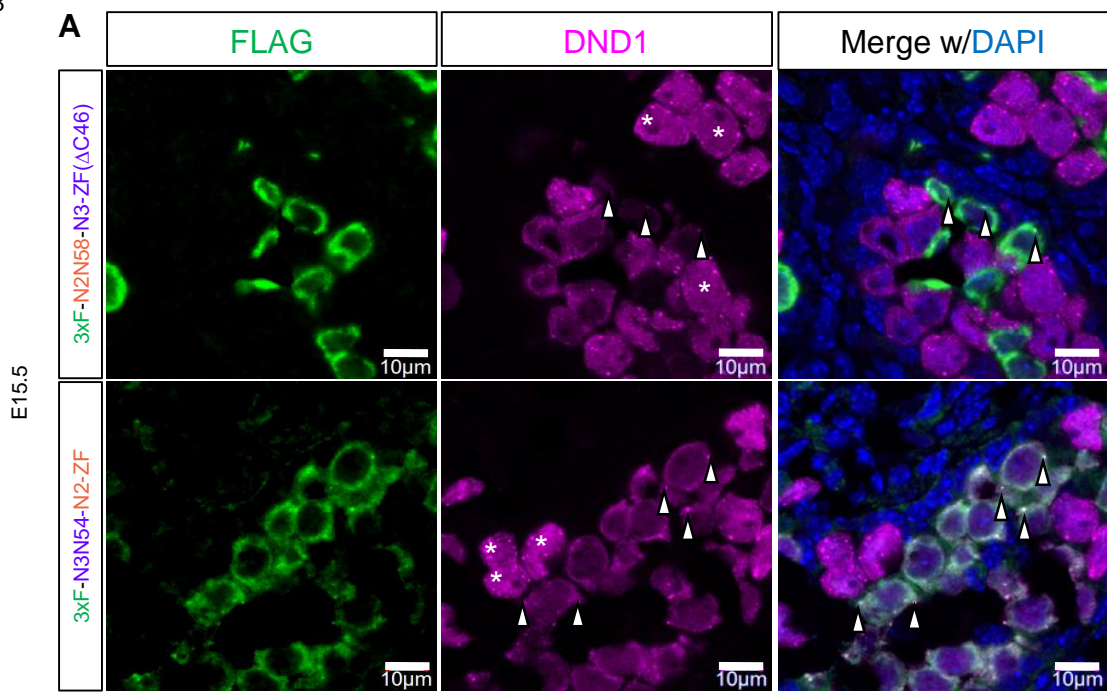
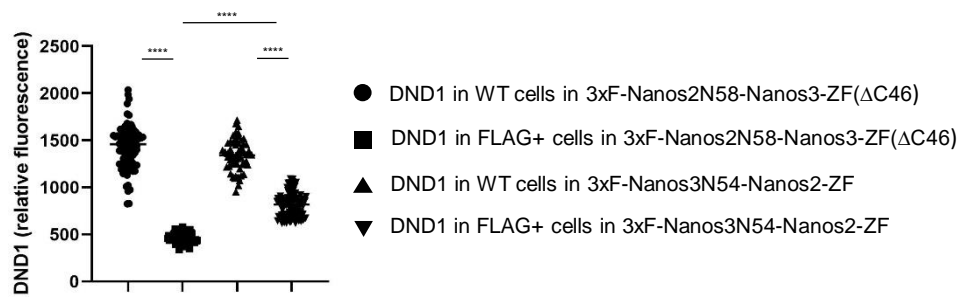


Figure 9

A



B

α -FLAG IP

HA-DND1		+	+	+	+	+	+
F	NANOS2	+	-	-	-	-	-
F	NANOS3	-	+	-	-	-	-
F	NANOS2-N58 NANOS3-ZF(Δ C46)	-	-	+	-	-	-
F	NANOS2-N58 NANOS3-full ZF	-	-	-	+	-	-
F	NANOS3-N54 NANOS2-ZF	-	-	-	-	+	-
F	NANOS2 NANOS3-C	-	-	-	-	-	+

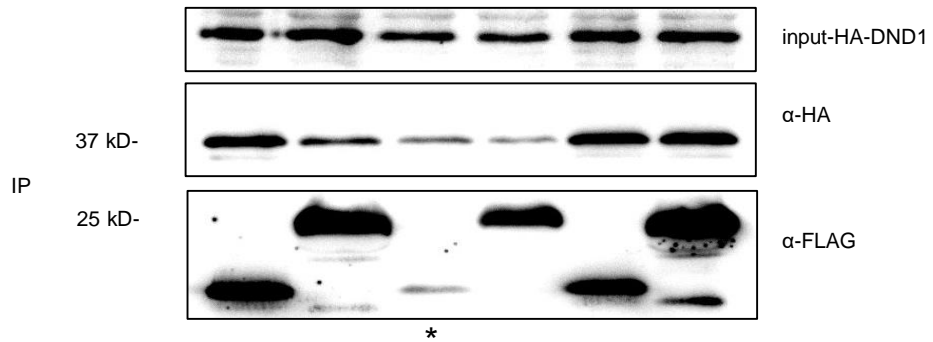


Figure 10

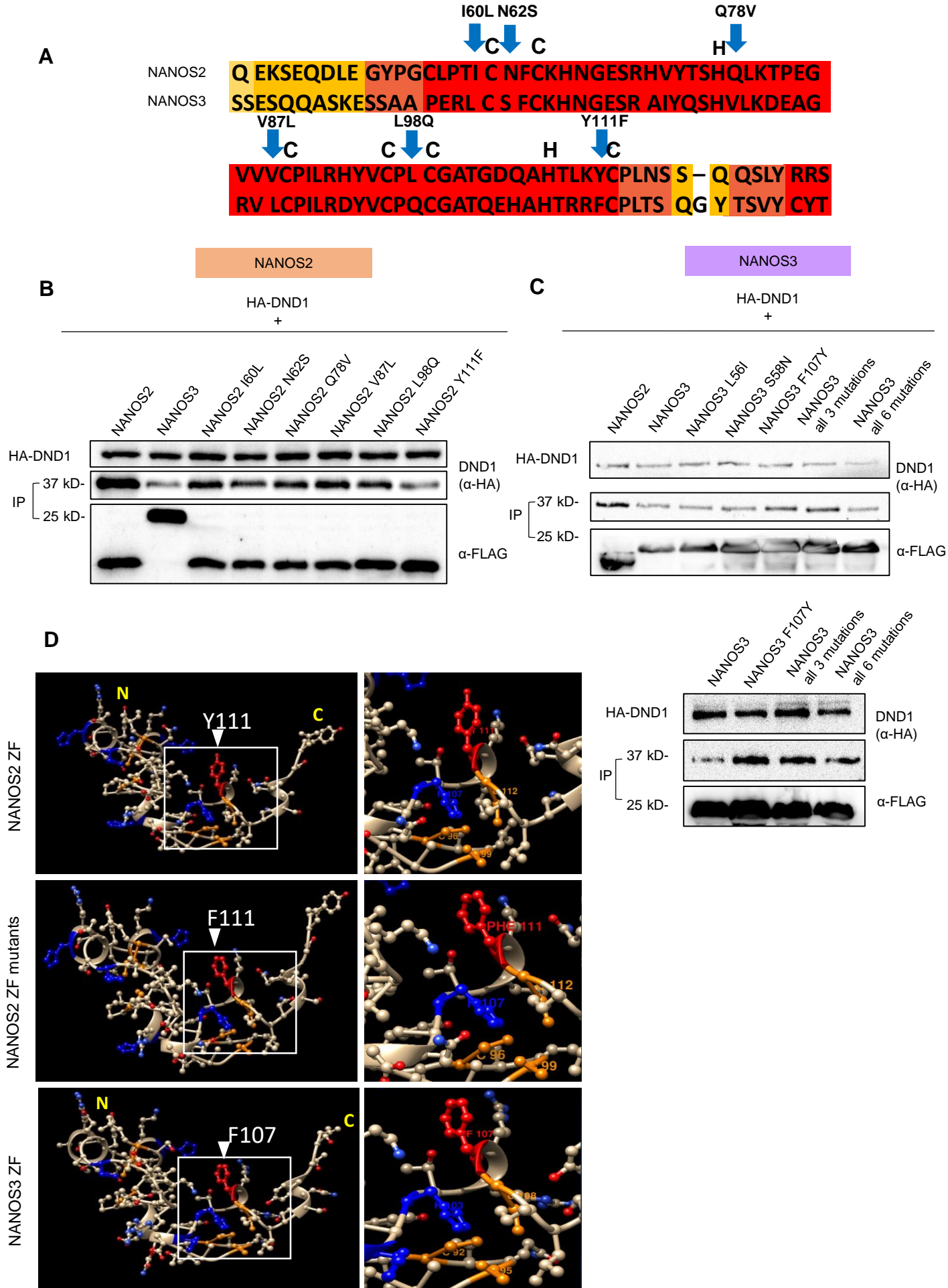


Figure 11

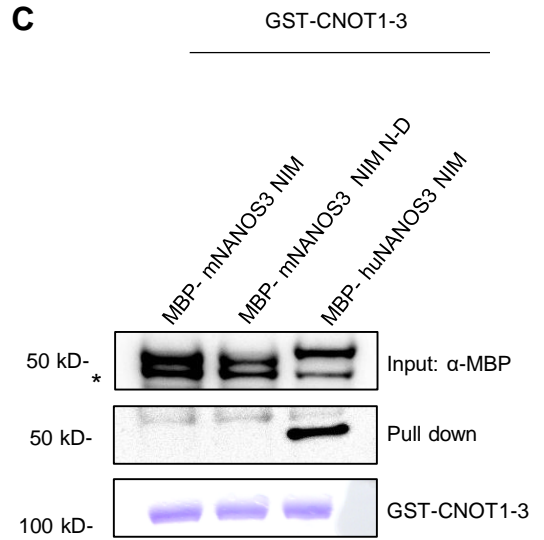
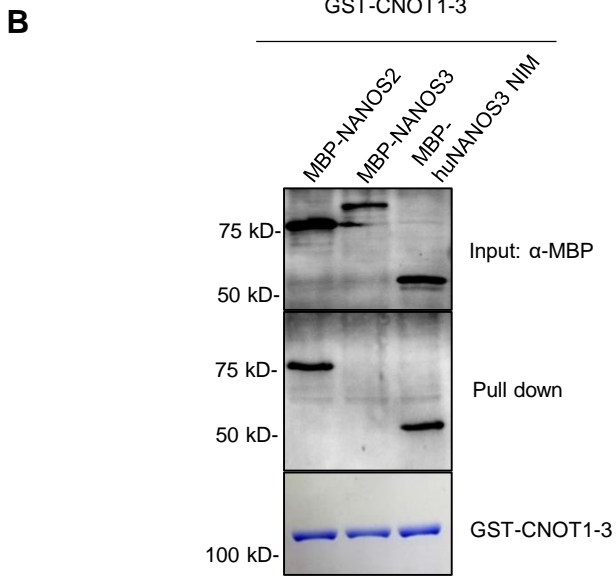
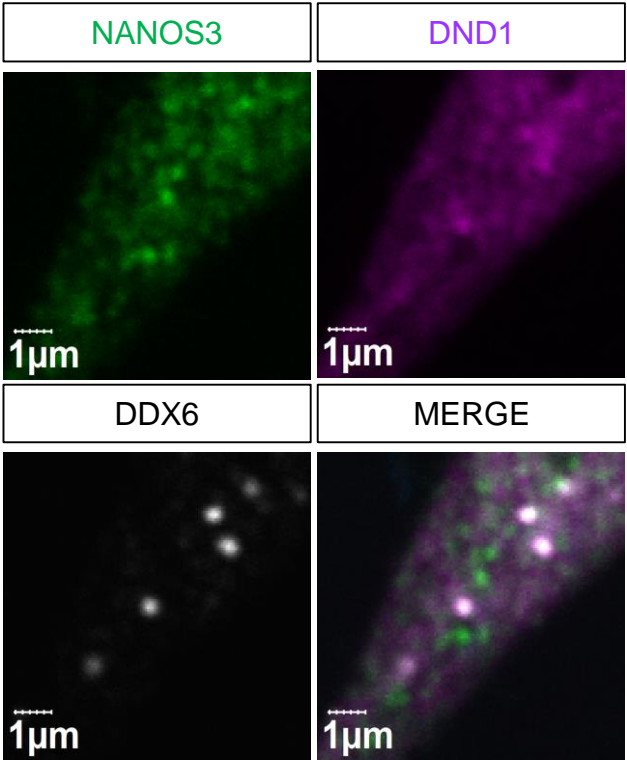
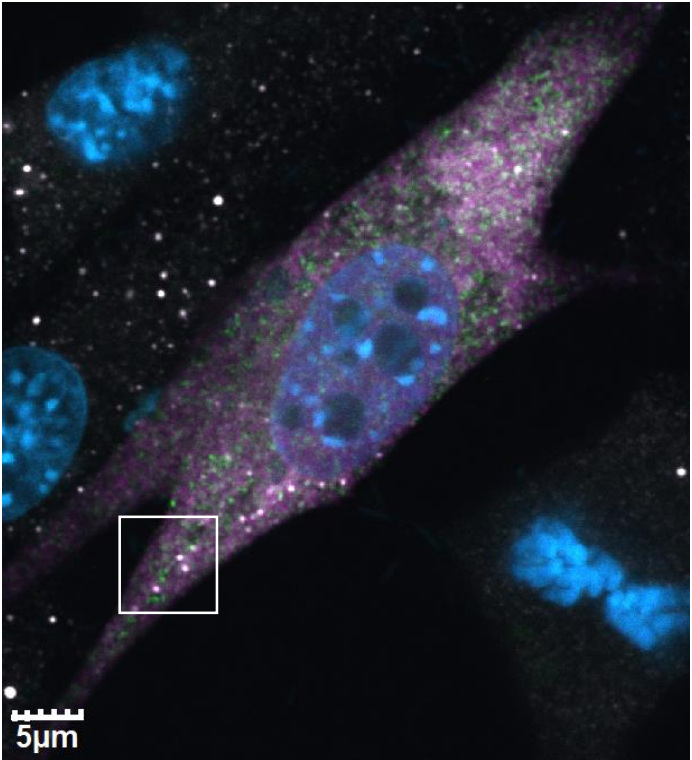


Figure 12

A

NANOS3/DND1/DDX6/DAPI



B

E15.5

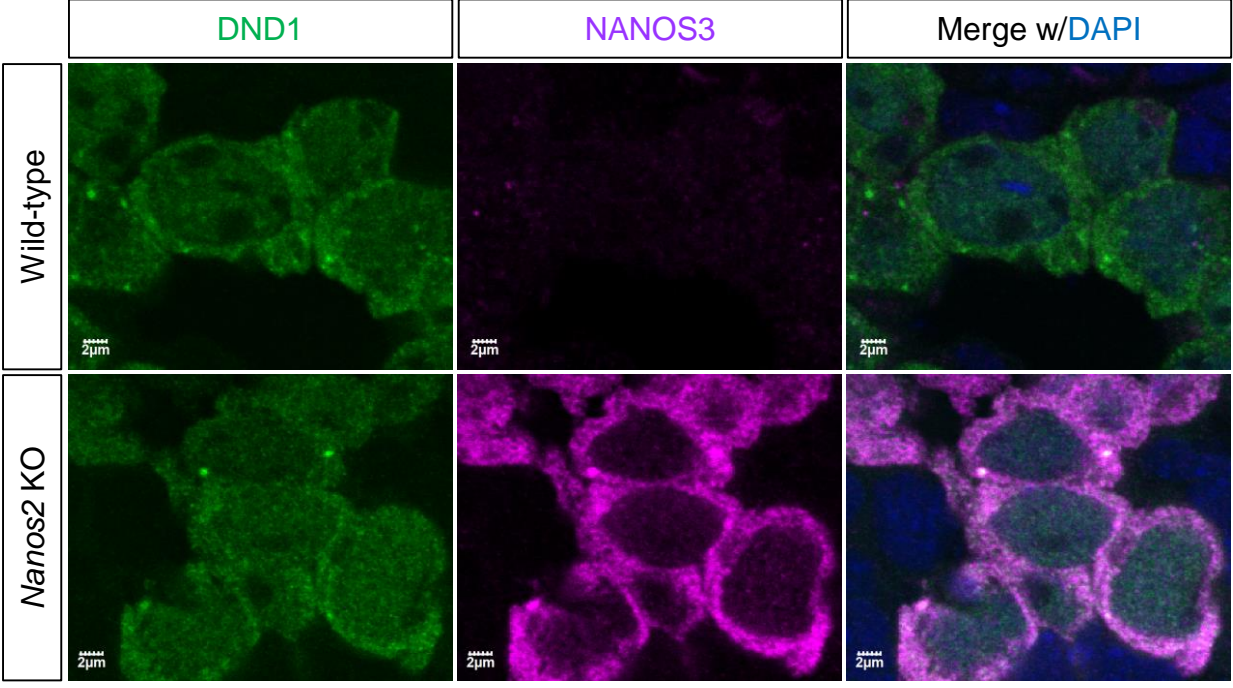


Figure 13

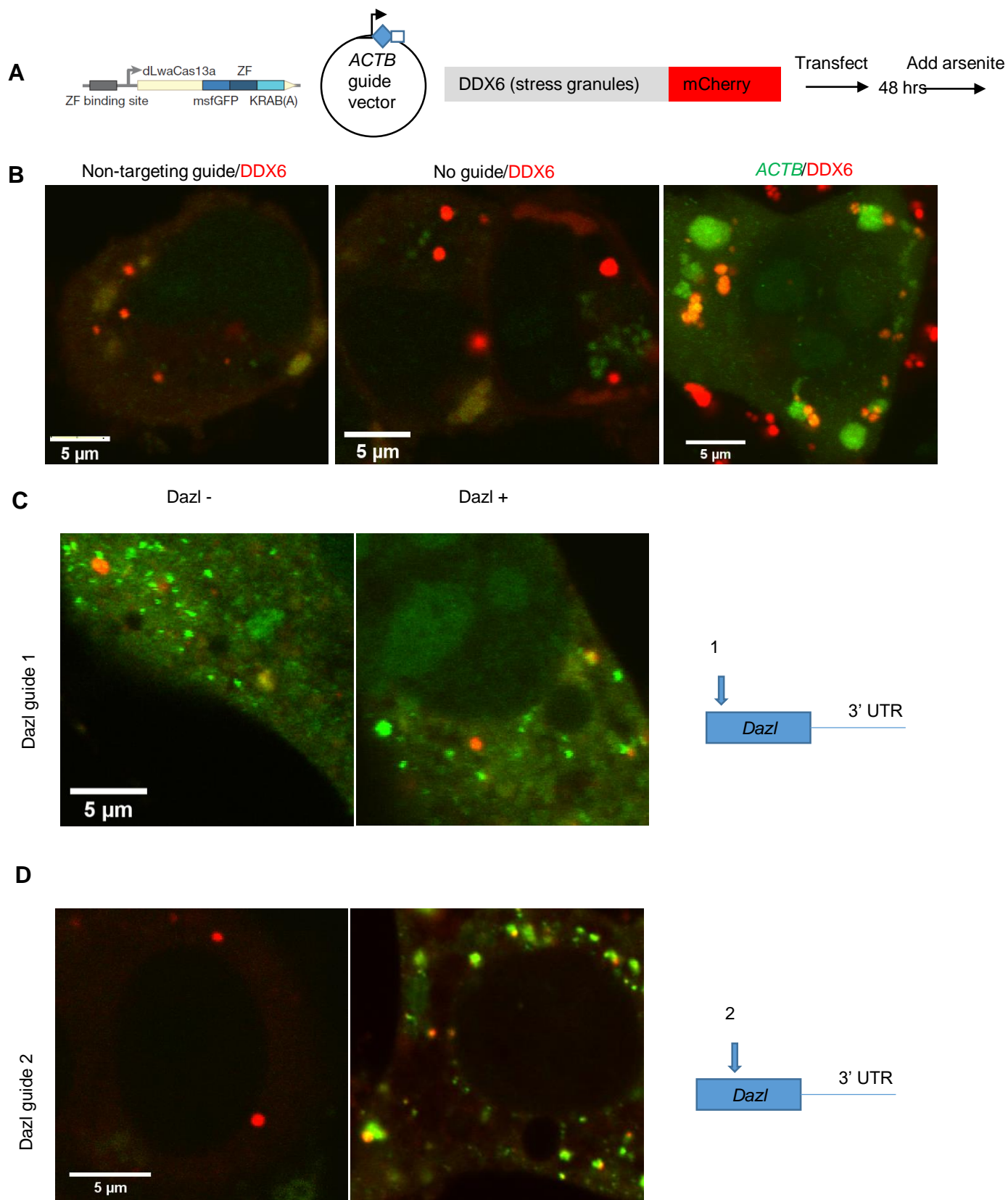


Figure 14

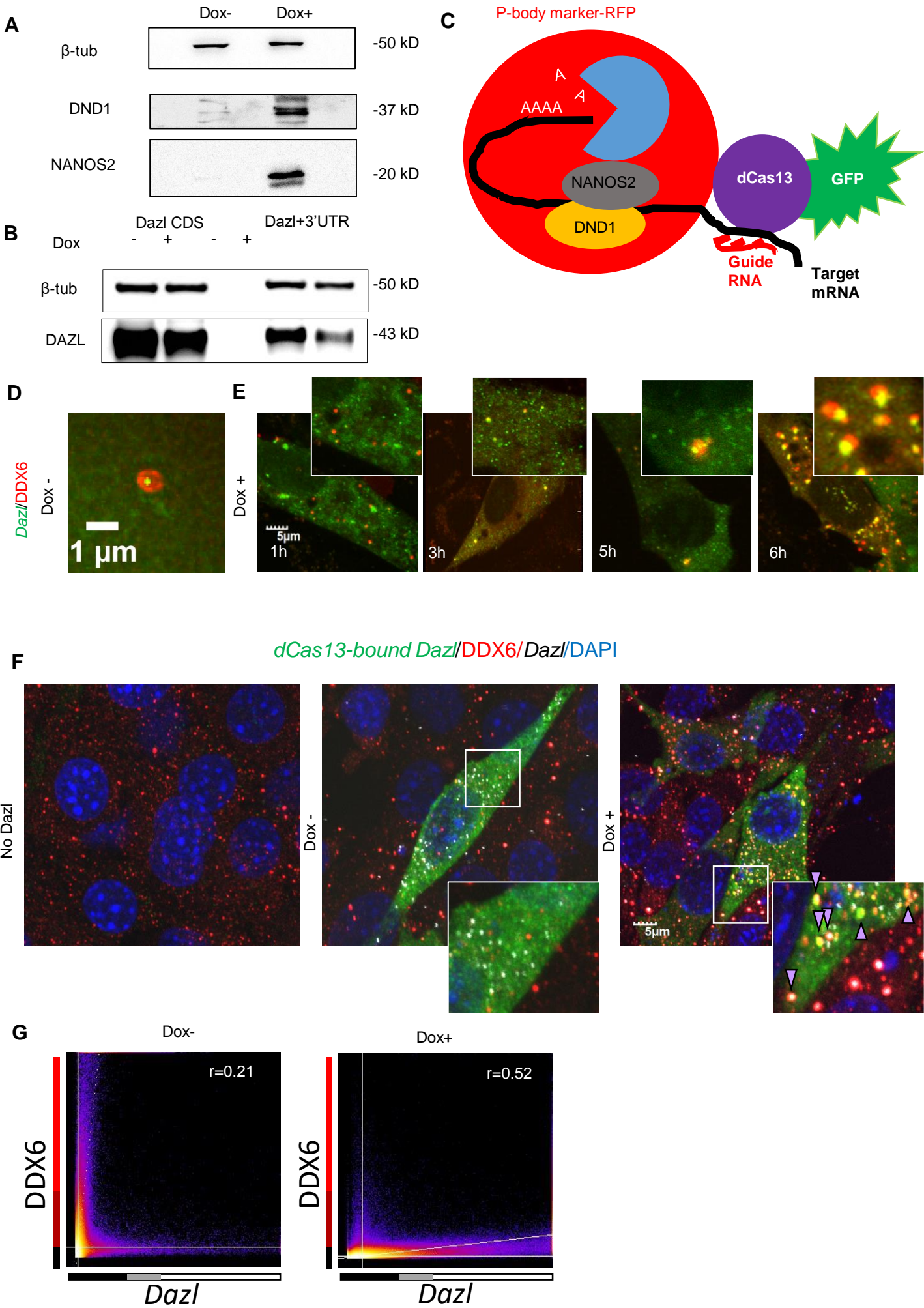
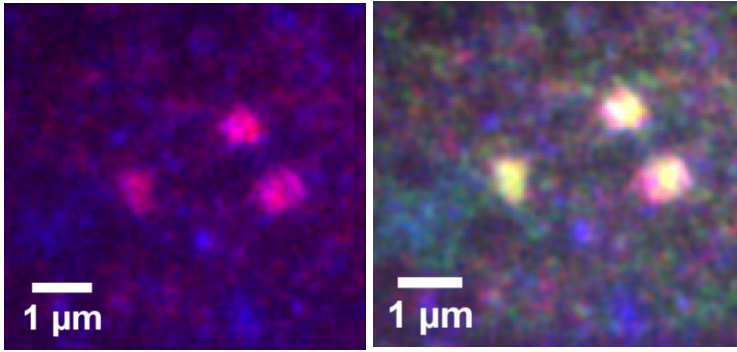


Figure 15

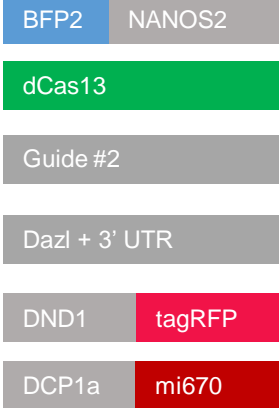
NANOS2/DND1

NANOS2/DND1/*Dazl*

A



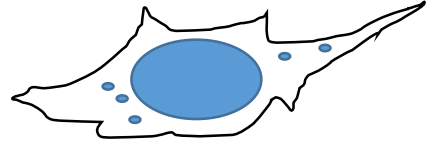
B



Transfect

24-48 hrs

Image

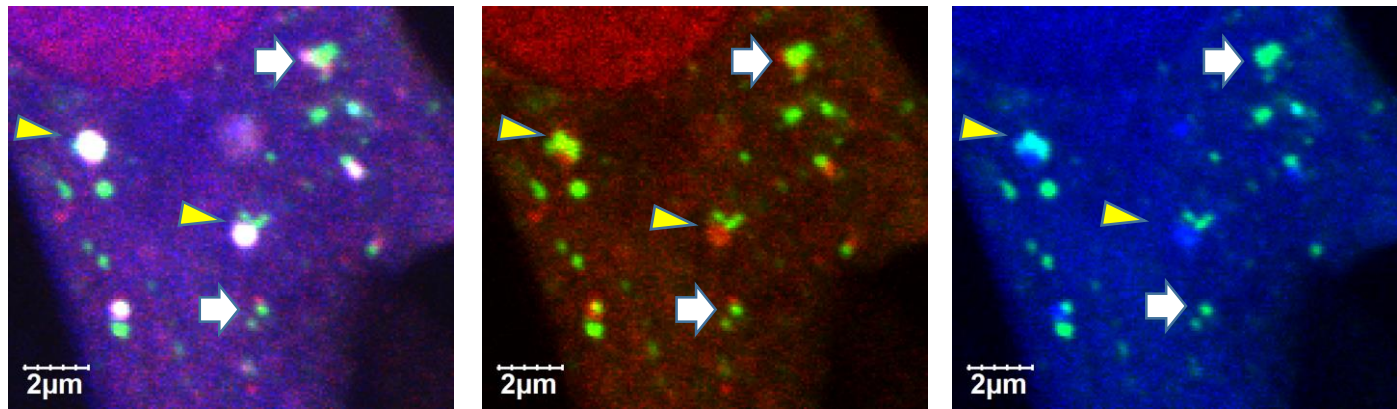


C

NANOS2/DND1/DCP1a/*Dazl*

DND1/*Dazl*

NANOS2/*Dazl*



D

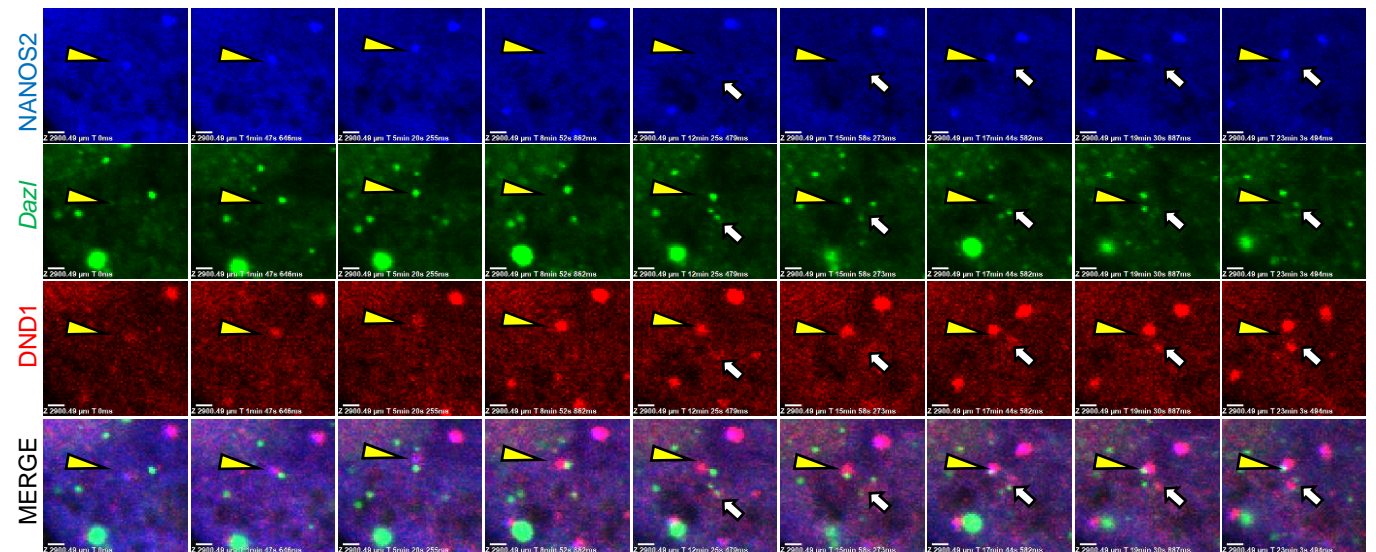
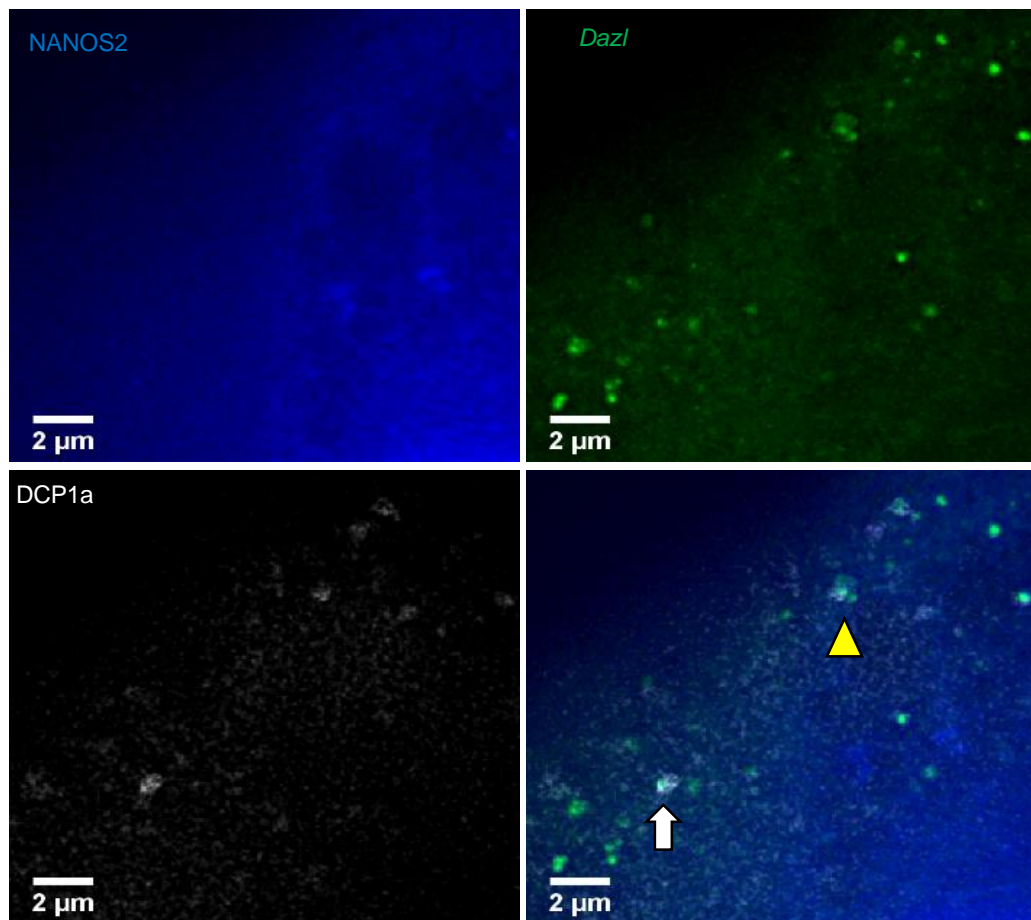


Figure 16

A



B

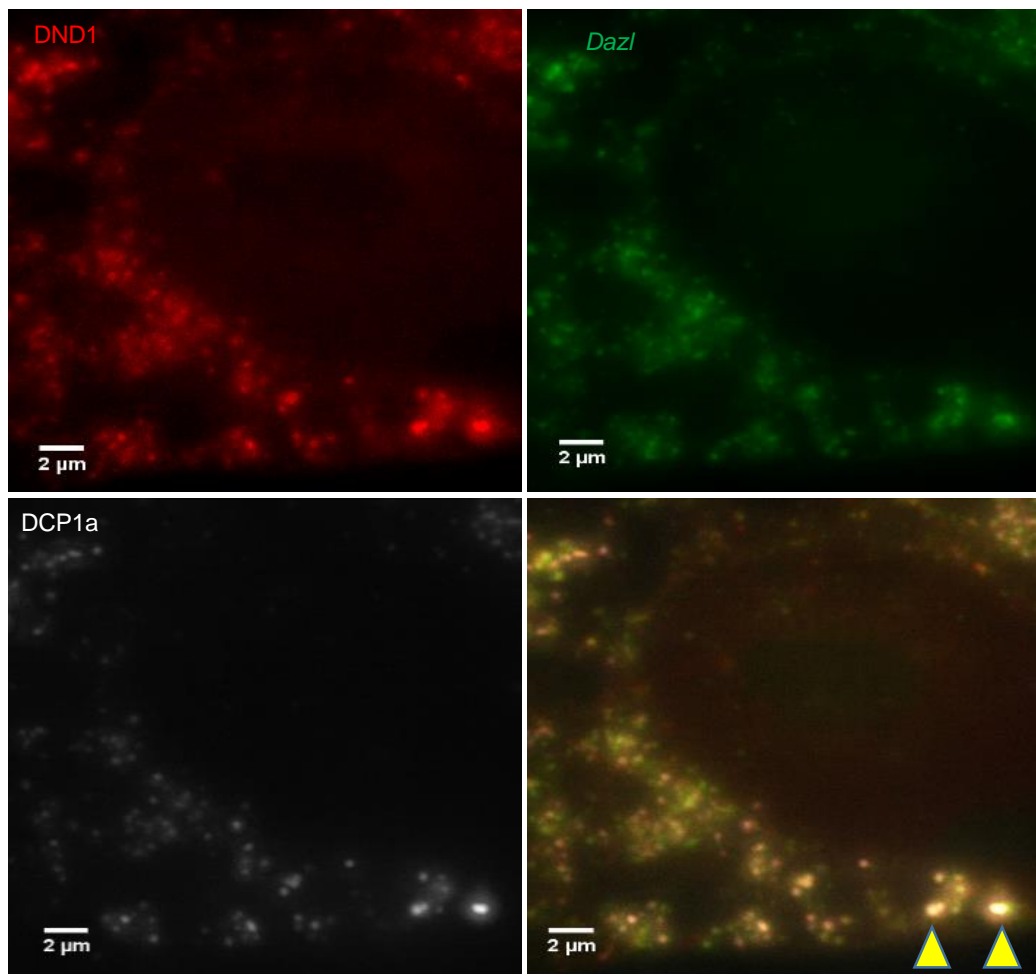
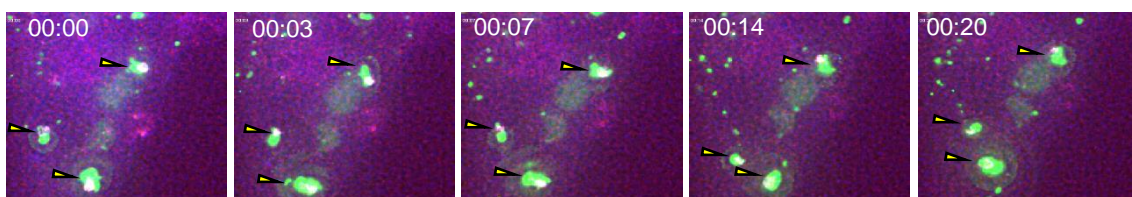
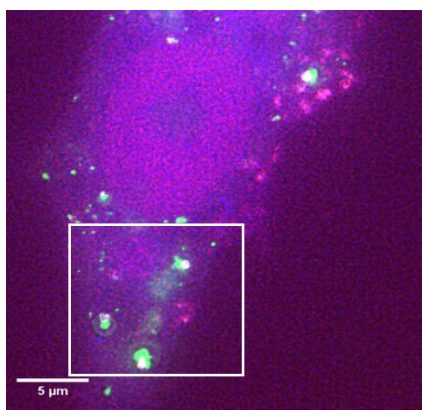
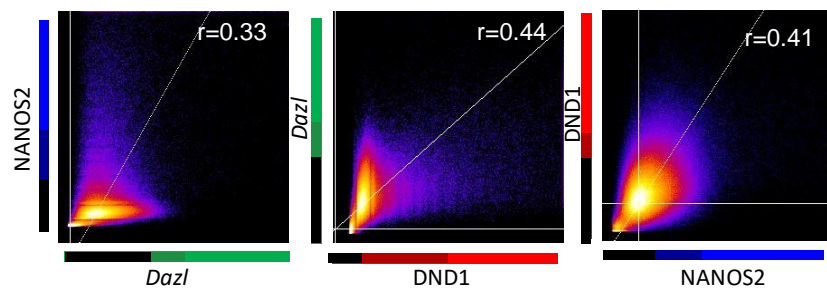


Figure 17

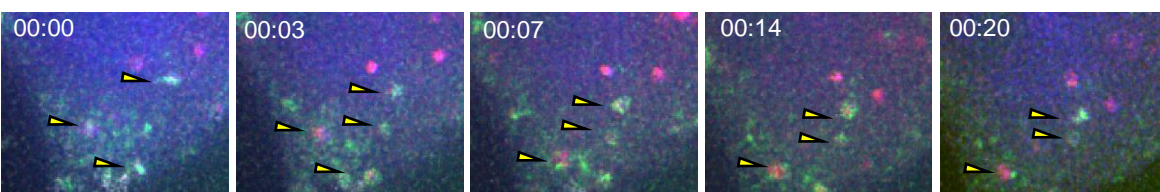
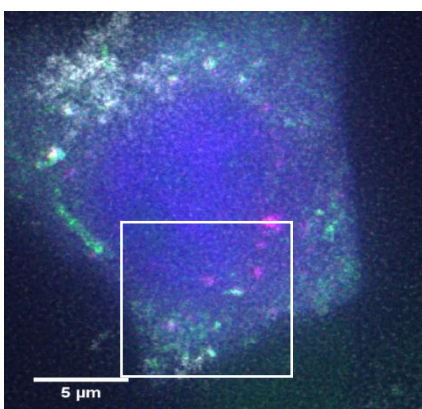
A

NANOS2/DND1/DCP1a/*Dazl*

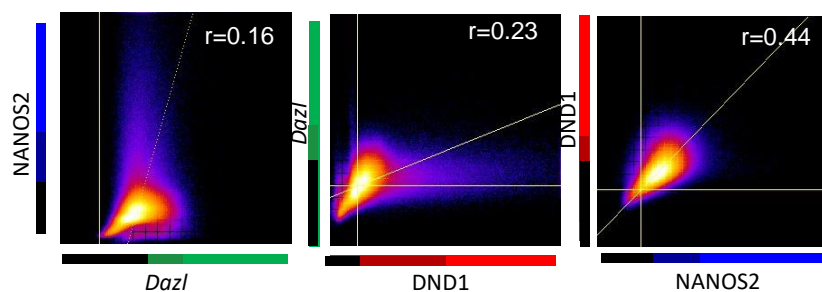
B



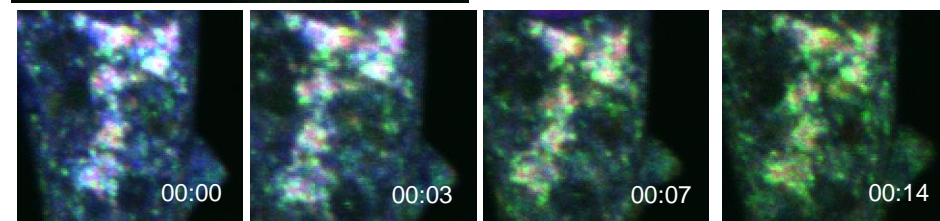
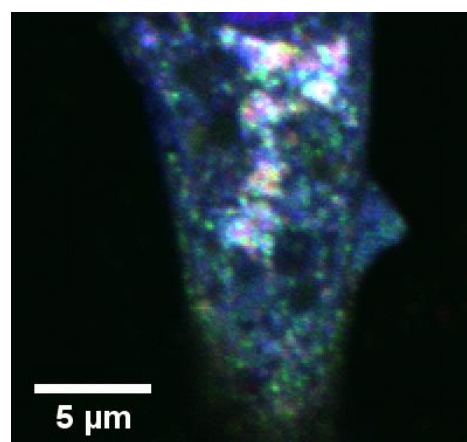
C

NANOS2/DND1R98A/DCP1a/*Dazl*

D



E

NANOS2-zm/DND1/*Dazl*

F

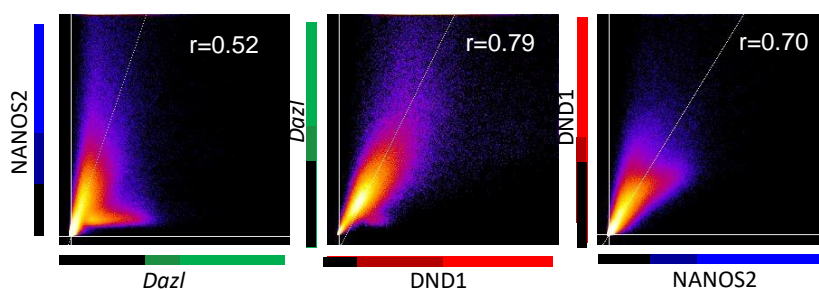


Figure 18

